Supplementary Information

CONTENTS

LIST OF TABLES:

LIST OF FIGURES:

A. EXPERIMENTAL

Materials and methods

For materials syntheses: EPDM-10-1000-AW (EPDM, 99.99 %, AGC SI-Tech Co, Ltd), LFS-HN-050 (LFS50, >98 %, AGC), LFS-HN-150 (LFS150, >98 %, AGC), tetra-*n*-propylammonium hydroxide (TPAOH, 40 wt% in water, Alfa Aesar), deionised water, sodium hydroxide pellets (99 %, Jose Manuel Gomes dos Santos, LDA), hydrogen peroxide (30 wt% in water, Puriss p.a Sigma-aldrich), hydrochloric acid (37 wt% in water, Puriss p.a Sigma-aldrich), hafnium(IV) acetylacetonate ($Hf(acac)_4$; 97 %, Alfa aesar), hafnium(IV) oxide (99.95 %, Alfa aesar). For catalytic tests: levulinic acid (98 %, Aldrich), 2-butanol (>99.5 %, Sigma-Aldrich).

Materials characterisation

The PXRD data were collected on an Empyrean PANalytical diffractometer (Cu-Ka X-radiation, K = 1.54060 Å) in a Bragg-Brentano para-focusing optical configuration (45 kV, 40 mA) at ambient temperature. The sample was prepared in a spinning flat plate sample holder and step-scanned in the 2θ range from 3-68° with steps of 0.026°. A PIXEL linear detector with an active area of 1.7462° was used with a counting time of 68 s per step.
Scanning electron microscope (SEM) images, elemental mappings (Si, Hf) and energy dispersive X-ray spectroscopy (EDS) images were obtained on a Hitachi SU-70 SEM microscope with a Bruker Quantax 400 detector operating at 15 kV. Samples were prepared by deposition on aluminium sample holders followed by carbon coating using an Emitech K 950 carbon evaporator. Scanning transmission electron microscopy images (STEM) were collected using a Hitachi HD 2700 scanning transmission electron microscope, equipped with a Bruker EDS detector. The samples were prepared by depositing a drop of an ethanol suspension of the sample onto holey amorphous carbon film coated 400 mesh copper grid (Agar Scientific).
Elemental analysis for C was performed on a Leco TruSpec 630-200-200 analyzer. Thermogravimetric analyses were carried out on a SETSYS Evolution 170 Setaran device by heating the samples to 800 °C (10 °C min^{-1}) under nitrogen flow. under N_2 flow (20 mL min^{-1}).
The N_2 sorption isotherms were measured at -196 °C, using a QuantaChrome Autosorb iQ2 Automated Gas Sorption analyser. The samples were pre-treated at 250 °C for 3 h, under vacuum (<4 x 10^{-3} bar). The specific surface area was calculated using the Brunauer, Emmett, Teller equation (S_{BET}). and mesopore sizes (d_p) were calculated using the DFT method; reliable results of total pore volume were not possible to determine due to the steep N_2 uptake as the relative pressure (p/p_0) approached unity. For commercial EPDM, the macropore size distribution was measured by Hg intrusion using a Micromeritics equipment, model AutoPore IV 9500 V1.09 Serial 622 (Norcross, Georgia, USA) (0.03-2275 bar); the sample was degassed, under vacuum at 6.58×10^{-5} bar, at room temperature.
^{29}Si MAS NMR spectra were recorded at 79.495 MHz on a Bruker Avance III 400 MHz spectrometer (9.4 T), using a 7 mm double resonance MAS probe, with 2.4 μs radiofrequency pulse (40 ° flip angle pulse), a recycle delay of 60 s, and 5 kHz spinning. Cross polarization (CP) $^{29}Si\{^1H\}$ CP MAS NMR spectra were measured with a 3.5 ms 1H 90º flip angle pulse, 8000 ms contact time, recycle delay of 5 s and 5 kHz spinning rate. Chemical shifts are quoted in ppm from tetramethylsilane (TMS). The ratio of silanols to siloxane (Q^4) groups, was calculated via spectral deconvolution (^{29}Si MAS NMR), using the following equation: $(2\times\%Q^2 + \%Q^3)/(\%Q^4)$ where $\%Q^n$ is the relative population of species Q^n (n = 2, 3, 4). The concentration of silanol groups (mol g^{-1}) was calculated using the following equation:[1] [SiOH] (expressed as mmol g^{-1}) = $1000 \times [(2\times\% Q^2) + \%Q^3]/[(\%Q^2 \times M_{(Si(OH)2(O))}) + (\%Q^3 \times M_{Si(OH)(O)1.5}) + (\%Q^4 \times M_{Si(O)2})]$, where M_i = molar mass of species *i* (silanol, geminal or siloxane).
X-ray photoelectron spectroscopy (XPS) analysis was performed using a Thermo Scientific ESCALAB 250Xi spectrometer equipped with a monochromatic Al Kα radiation ($h\nu$ = 1486.6 eV) as excitation source. The 20-eV pass energy value of a hemispherical electron energy analyser

was used for the high-resolution spectra acquisition. The energy scale of the system was calibrated with respect to Au $4f_{7/2}$, Ag $3d_{5/2}$ and Cu $2p_{3/2}$ peak positions. ESCALAB 250Xi Avantage software was used for the peak deconvolution. All spectra fitting procedures were performed using symmetrical peaks and 70:30 Gauss-Lorentz function ratio.
Attenuated total reflectance (ATR) Fourier-transform infrared FT-IR spectra were recorded on a Unican Mattson Mod 7000 spectrometer equipped with a Specac Golden Gate Mk II ATR accessory fitted with a diamond top plate and KRS-5 focusing lenses (400-4000 cm^{-1}, 256 scans, 4 cm^{-1} resolution). Diffuse reflectance UV-vis spectra were recorded on a Jasco V-780 spectrophotometer using an integrating sphere of 60 mm coated with barium sulfate with light detection source D2/WI by a photomultiplier tube (ISV-922/ISN-923/ISN-901i) attached to the base of the sphere in reflectance photometric mode with a wavelength scan speed of 100 nm min^{-1} in the range 190-900 nm, data interval of 0.5 nm and a bandwidth of 2.0 nm.
The acid properties were measured using a Nexus Thermo Nicolet apparatus (64 scans and resolution of 4 cm^{-1}) equipped with a specially designed cell, using self-supported discs (5-10 mg cm^{-2}) and pyridine as base probe. After *in situ* outgassing at 450 °C for 3 h under vacuum (10^{-6} mbar), the sample was contacted with pyridine (99.99 %) at 150 °C for 10 min, and subsequently evacuated at 150 and 350 °C for 30 min, under vacuum. The quantitative measurements were based on the areas of the bands at *ca.* 1540 and 1430-1460 cm^{-1} which are associated with pyridine adsorbed on Brønsted (B) and Lewis (L) acid sites, respectively, and using molar extinction coefficients determined in the home-made IR installation used (1.58 and 0.9 cm/μmol for L and B acid sites, respectively). The L and B acid strengths were based on the molar ratio of acid sites measured after evacuation at 150 and 350 °C (L_{350}/L_{150} and B_{350}/B_{150}, respectively); it is reasonable to consider that the acid sites of moderate strength remain adsorbed at 150 °C, and relatively strong acid sites remain adsorbed at 350 °C.

B. KINETIC MODELING

The modelling was carried out in MatLab (version 9.14), considering a perfectly stirred, isothermal batch reactor, with material balances given by equation (1),

$$\frac{V}{W}.\frac{dC_i}{dt} = r_i \tag{1}$$

where V is the volume of the reaction mixture (L), W is the mass of catalyst (g), C_i is the molar concentration of species *i* (M), t is the reaction time (h) and r_i is the reaction rate of species *i* (mol g_{cat}^{-1} h^{-1}); the V/W ratio was kept constant in all experiments. A pseudo-homogeneous model was developed considering irreversible and first order reactions, according to the ordinary differential equations (2) - (5). The system of equations was solved by numerical integration with optimisation, using appropriate initial conditions and the adjustment was made by minimising the objective function (F_{obj}), which gave the kinetic constants (ki).

$$\frac{V}{W}\frac{dC_{LA}}{dt} = -\left(k_1 + k_3 + k_4\right) C_{LA} \tag{2}$$

$$\frac{V}{W}\frac{dC_{2BL}}{dt} = k_1 C_{LA} - k_2 C_{2BL} \tag{3}$$

$$\frac{V}{W}\frac{dC_{GVL}}{dt} = k_2 C_{2BL} + k_3 C_{LA} \tag{4}$$

$$\frac{V}{W}.\frac{dC_{D_{LA}}}{dt} = k_4 . C_{LA} \tag{5}$$

$$F_{obj} = \sum_{m} \left[\sum_{n=1}^{n_p} \left(C_{m,n}|_{cal} - C_{m,n}|_{exp} \right)^2 \right] \quad (6)$$

where $Cm,n|calc$ is the concentration predicted by the model and $Cm,n|exp$ is the experimental concentration value for each experimental point n (corresponding to different reaction times) and each species m (m = LA, 2BL, GVL or DLA (by-products)).

C. CHARACTERISATION

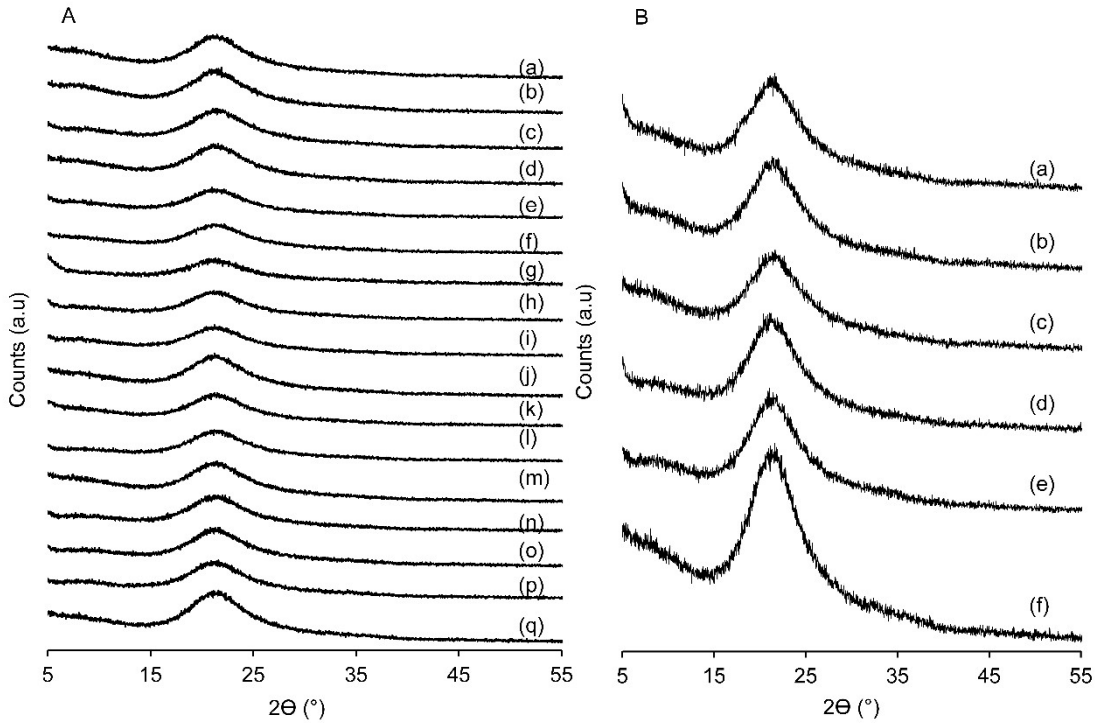

Figure S1. PXRD patterns of **(A)** H-EPDM-1.2TPA3 (a); EPDM-1.2TPA3 (b); H-EPDM-0.6TPA3 (c); EPDM-0.6TPA3 (d); H-EPDM-0.4TPA3 (e); EPDM-0.4TPA3 (f); H-EPDM-0.2TPA3-HCl (g); EPDM-0.2TPA3 (h); H-EPDM-0.2TPA1.5 (i); EPDM-0.2TPA1.5 (j); H-EPDM-0.08TPA3 (k); EPDM-0.08TPA3 (l); H-EPDM-0.08TPA1.5 (m); EPDM-0.08TPA1.5 (n); EPDM-0.08TPA0.5 (o); EPDM-0.04TPA0.5 (p); EPDM (q). **(B)** H-EPDM-0.2Na3 (a); EPDM-0.2Na3 (b); H-EPDM-0.2Na1.5 (c); EPDM-0.2Na1.5 (d); EPDM-0.2Na0.5 (e); EPDM (f).

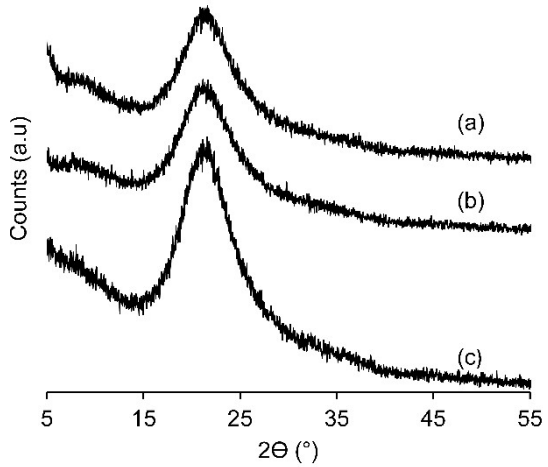

Figure S2. PXRD patterns of EPDM-HT-4.5 (a); EPDM-HT-1.5 (b) and EPDM (c).

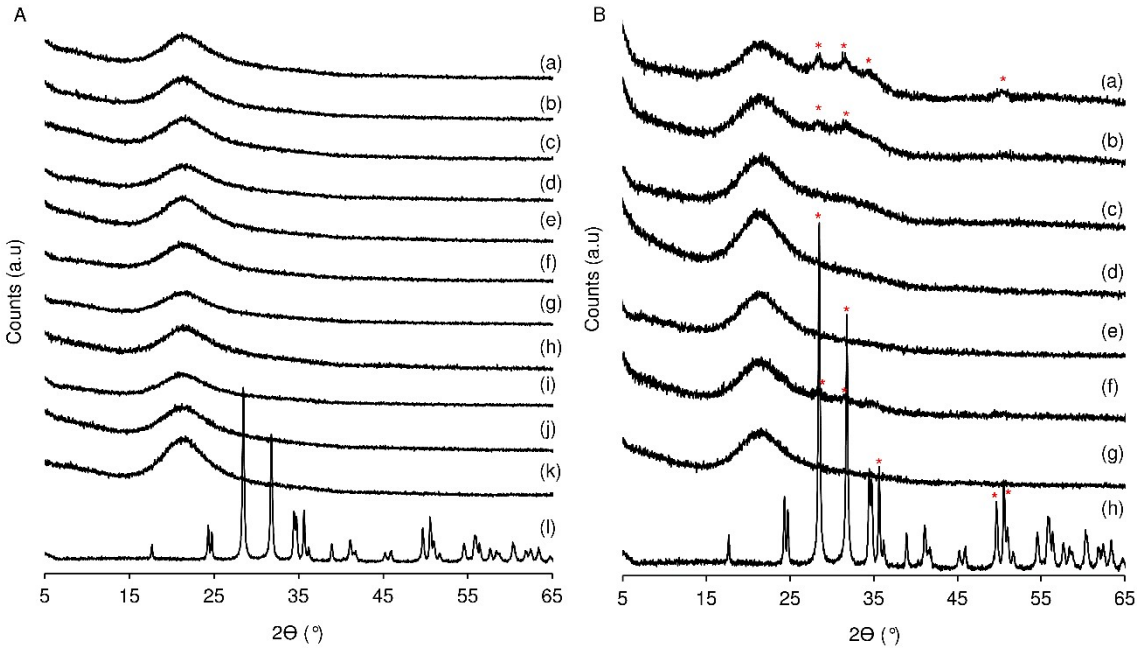

Figure S3. PXRD patterns of **(A)** 2Hf-EPDM-1.2TPA (WI (a); SS (b)); 2Hf-EPDM-0.6TPA (WI (c); SS (d)); 2Hf-EPDM-0.4TPA (WI (e); SS (f)); 2Hf-EPDM-0.2TPA (WI (g); SS (h)); 2Hf-EPDM-0.08TPA (WI (i); SS (j)); EPDM (k); and HfO_2 (l). **(B)** wHf-EPDM-SS (w = 16 (a); 12 (b); 8 (c); 4 (d); 2(e)); wHf-EPDM-WI (w = 8 (f); 2 (g)); and HfO_2 (h). The red asterisks signalise peaks associated with HfO_2.

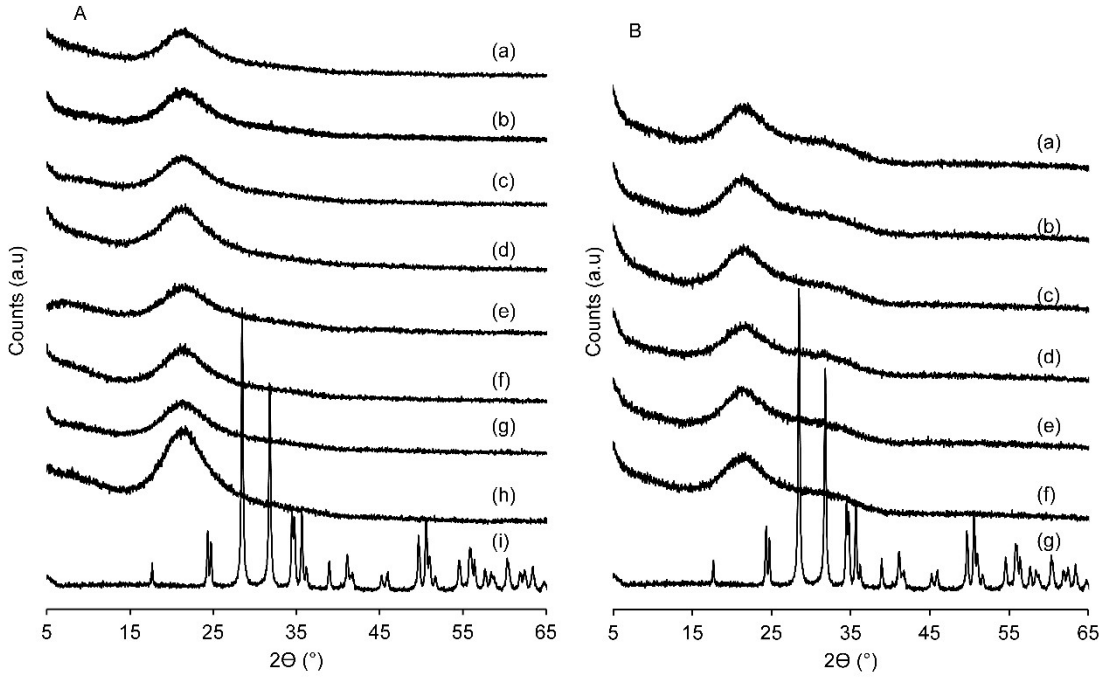

Figure S4. PXRD patterns of **(A)** 2Hf-EPDM-HT4.5 (WI (a);SS (b)); 2Hf-EPDM-HT1.5-SS (c); 2Hf-EPDM-0.2Na3 (WI (d); SS (e)); 2Hf-EPDM-0.2Na1.5 (WI (f); SS (g)); EPDM (h); and HfO_2 (i). **(B)** 8Hf-EPDM-HT4.5-SS (a); 8Hf-EPDM-0.2Na3-SS (b); 8Hf-EPDM-1.2TPA3-SS (c); 8Hf-

EPDM-0.6TPA3-SS (d); 8Hf-EPDM-0.4TPA3-SS (e); 8Hf-EPDM-0.2TPA3-SS (f); and HfO_2 (g).

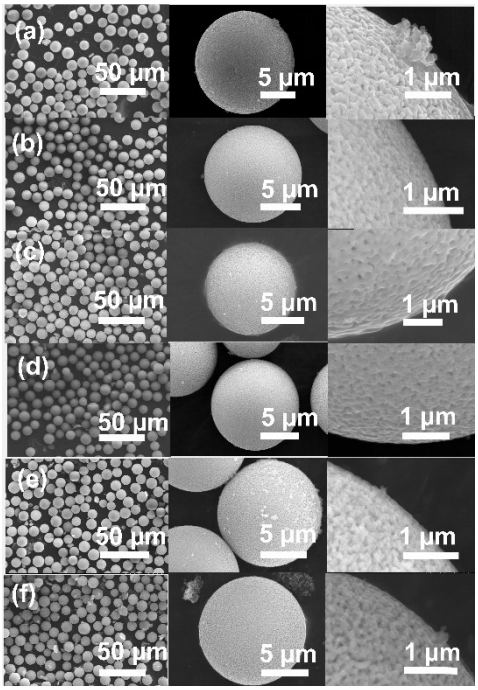

Figure S5. SEM images of (a) EPDM, (b) EPDM-HT4.5, (c) EPDM-0.08TPA3, (d) H-EPDM-0.08TPA3, (e) EPDM-0.24TPA3 and (f) H-EPDM-0.24TPA3.

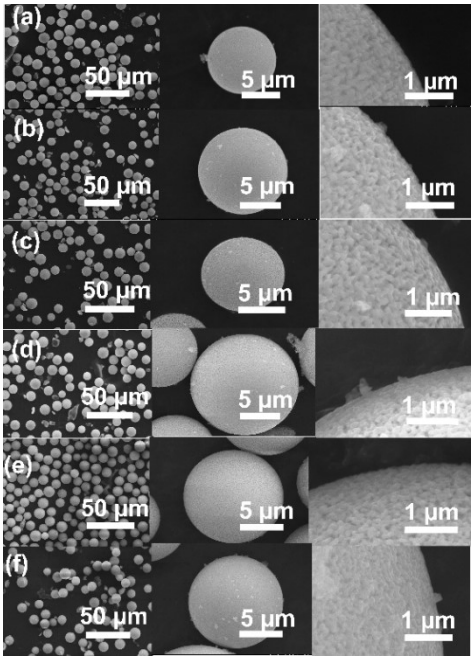

Figure S6. SEM images of (a) EPDM-0.4TPA3, (b) H-EPDM-0.4TPA3, (c) EPDM-0.6TPA3, (d) H-EPDM-0.6TPA3, (e) EPDM-1.2TPA3 and (f) H-EPDM-1.2TPA3.

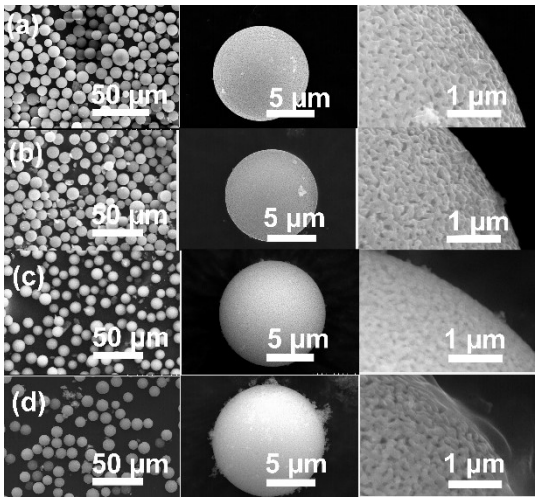

Figure S7. SEM images of (a) EPDM-0.2Na1.5, (b) H-EPDM-0.2Na1.5, (c) EPDM-0.2Na3 and (d) H-EPDM-0.2Na3.

Table S1. Composition and textural properties of the EPDM based silicas.

Sample	**Si/Hf (synth)[a]**	**Si/Hf (EDS)[a]**	**S_{BET} (m^2 g^{-1})**	**d_p (nm)**
EPDM (comercial)		-	57	2-10[b]
2Hf-EPDM-SS	149	151	122	2-10
2Hf-EPDM-WI	149	138	77	2-10
4Hf-EPDM-SS	74	79	-	-
8Hf-EPDM-SS	37	34	117	2-12
8Hf-EPDM-WI	37	40	109	2-10
12Hf-EPDM-SS	25	28	-	-
16Hf-EPDM-SS	19	24	-	-
EPDM-HT1.5	-	-	35	2-10
2Hf-EPDM-HT1.5-SS			122	2-12
2Hf-EPDM-HT1.5-WI			103	3-13
EPDM-HT4.5	-	-	31	5-18
2Hf-EPDM-HT4.5-SS	141	-	142	3-15
2Hf-EPDM-HT4.5-WI	141	-	83	4-15
8Hf-EPDM-HT4.5-SS	35	42	119	2-12
EPDM-0.04TPA0.5	-	-	64	2-15
EPDM-0.08TPA0.5	-	-	61	2-15
EPDM-0.08TPA1.5	-	-	62	2-12
H-EPDM-0.08TPA1.5			134	4-16
EPDM-0.08TPA3	-	-	71	2-10
H-EPDM-0.08TPA3			95	2-18
2Hf-EPDM-0.08TPA-SS			142	3-12
2Hf-EPDM-0.08TPA-WI			109	3-14
EPDM-0.2TPA1.5	-	-	76	3-13
H-EPDM-0.2TPA1.5			153	2-10
EPDM-0.2TPA3	-	-	71	2-10
H-EPDM-0.2TPA3	-	-	96	2-19
2Hf-EPDM-0.2TPA-SS	147	-	116	2-10
2Hf-EPDM-0.2TPA-WI	147	-	78	2-9
8Hf-EPDM-0.2TPA-SS	37	43	86	2-10
EPDM-0.4TPA3	-	-	80	2-12
H-EPDM-0.4TPA3			103	2-10

2Hf-EPDM-0.4TPA-SS			121	2-12
2Hf-EPDM-0.4TPA-WI			93	2-12
EPDM-0.6TPA3	-	-	86	2-8
H-EPDM-0.6TPA3			116	2-8
2Hf-EPDM-0.6TPA-SS			121	4-16
2Hf-EPDM-0.6TPA-WI			90	2-9
EPDM-1.2TPA3	-	-	149	4-18
H-EPDM-1.2TPA3			167	2-10
2Hf-EPDM-1.2TPA-SS			100	2-9
2Hf-EPDM-1.2TPA-WI			65	3-10
EPDM-0.2Na0.5	-	-	52	1-10
H-EPDM-0.2Na0.5			93	3-15
EPDM-0.2Na1.5	-	-	53	1-15
H-EPDM-0.2Na1.5			89	2-10
2Hf-EPDM-0.2Na1.5-SS			127	2-11
2Hf-EPDM-0.2Na1.5-WI			64	2-16
EPDM-0.2Na3	-	-	86	3-15
H-EPDM-0.2Na3	-	-	167	2-10
2Hf-EPDM-0.2Na3-SS	147	-	192	2-10
2Hf-EPDM-0.2Na3-WI	147	-	73	2-12
8Hf-EPDM-0.2Na3-SS	37	37	115	2-10

[a] Si/Hf molar ratio. Synth. = Si/Hf ratio based on the catalyst preparation conditions. EDS = Si/Hf ratio based on EDS measurements and considering the volatiles (water) content in the samples (measured by thermogravimetric analysis, TGA)). [b] Based on Hg intrusion, EPDM also possessed macroporosity (70-100 nm).

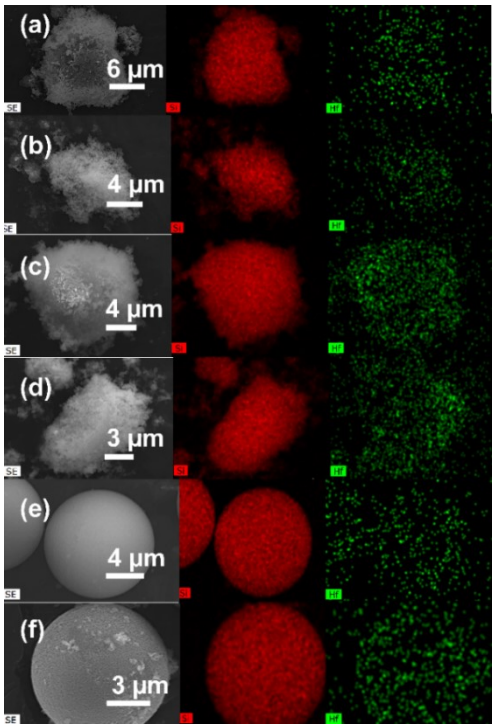

Figure S8. SEM images (a-d) and elemental mappings of Si (red) and Hf (green) for 2Hf-EPDM-SS (a), 8Hf-EPDM-SS (b), 12Hf-EPDM-SS (c), 16Hf-EDPM-SS (d), 2Hf-EPDM-WI (e) and 8Hf-EPDM-WI (f). No intense coloured regions were observed for all these samples, suggesting that they did not possess micron size particles.

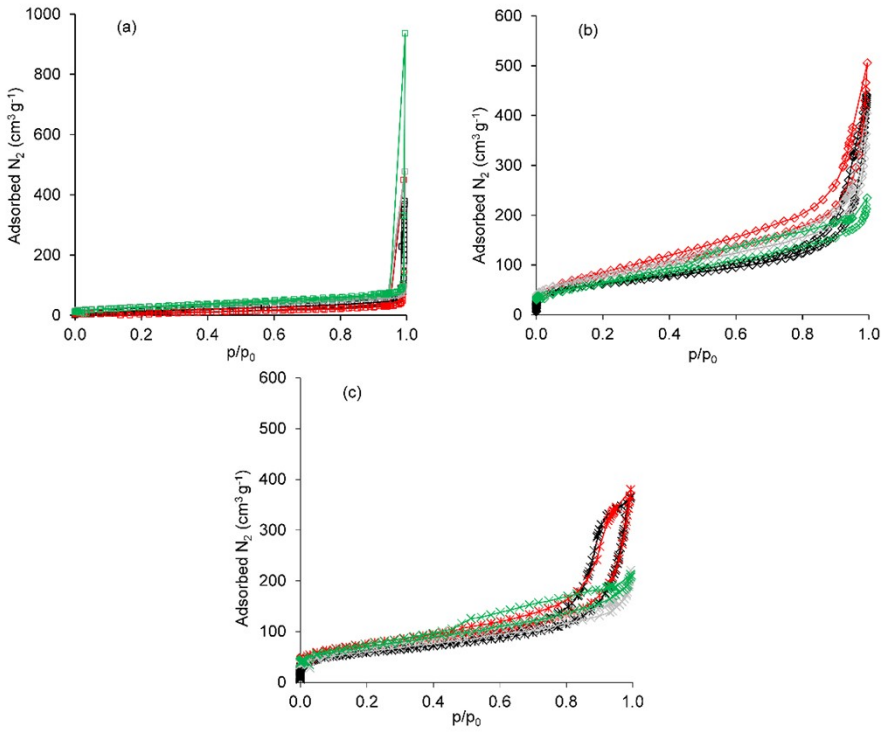

Figure S9. Nitrogen sorption isotherms at -196 °C for the EPDMs (a), LFS50s (b) and LFS150s (c). The black coloured curves are for the untreated (commercial) silicas, the red curves are for the correspondent HT-treated silica supports (EPDM-HT4.5, LFS50-HT, LFS150-HT), the grey curves are for the correspondent 0.2 M TPAOH treated silica supports (H-EPDM-0.2TPA3, H-LFS50-TPA, H-LFS150-TPA), and the green curves are for the correspondent 0.2 M NaOH treated silicas (H-EPDM-0.2Na3, H-LFS50-Na, H-LFS150).

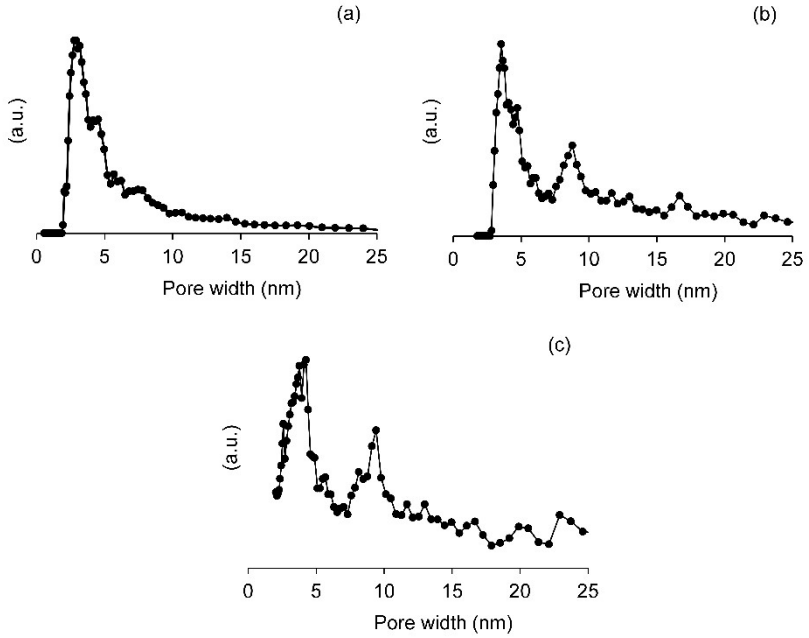

Figure S10. Pore size distribution (PSD) of commercial EPDM (a), LFS50 (b) and LFS150 (c), based on the DFT method (adsorption branch).

Table S2. The ratio $(2Q^2+Q^3)/Q^4$ and the concentration of SiOH groups of selected materials.

Sample	Q^1 [a]	Q^2 [a]	Q^3 [a]	Q^4 [a]	$(2Q^2+Q^3)/Q^4$	SiOH

	(%)	(%)	(%)	(%)		(mmol g^{-1}) [b]
EPDM	-	1.1	0.3	98.6	0.02	0.4
EPDM-HT4.5	-	2.4	0.6	97.0	0.05	0.9
H-EPDM-0.2TPA3	-	2.4	1.9	95.7	0.07	1.1
H-EPDM-0.2Na3	-	2.9	0.1	97.0	0.06	1.0
LFS150	.	1.0	7.3	91.7	0.10	1.5
LFS150-HT	-	1.2	7.6	91.2	0.11	1.6
H-LFS150-TPA	-	0.5	14.7	84.8	0.18	2.5
H-LFS150-Na	-	0.4	16.1	83.5	0.20	2.8
LFS50	0.6	1.0	7.6	90.8	0.11	1.6
8Hf-LFS50-SS	-	0.2	3.8	96.0	0.04	0.7
8Hf-LFS50-WI	-	0.1	1.1	98.8	0.01	0.2
LFS50-HT	-	0.7	7.9	91.4	0.10	1.5
8Hf-LFS50-HT-SS	-	0.9	4.1	95.0	0.06	1.0
8Hf-LFS50-HT-WI	-	0.5	1.6	97.9	0.03	0.4
H-LFS50-TPA	-	0.7	10.8	88.5	0.14	2.0
8Hf-LFS50-TPA-SS	-	0.2	2.8	97.0	0.03	0.5
8Hf-LFS50-TPA-WI	-	0.3	2.5	97.1	0.03	0.5
H-LFS50-Na	-	0.5	18.2	81.3	0.24	3.1
8Hf-LFS50-Na-SS	-	0.4	0.6	99.0	0.01	0.2
8Hf-LFS50-Na-WI	-	0.4	0.8	98.9	0.02	0.3

[a] Based on spectra deconvolution and integration. [b] Concentration of silanol groups, based on ^{29}Si MAS NMR spectroscopy (please see the above experimental section for details).

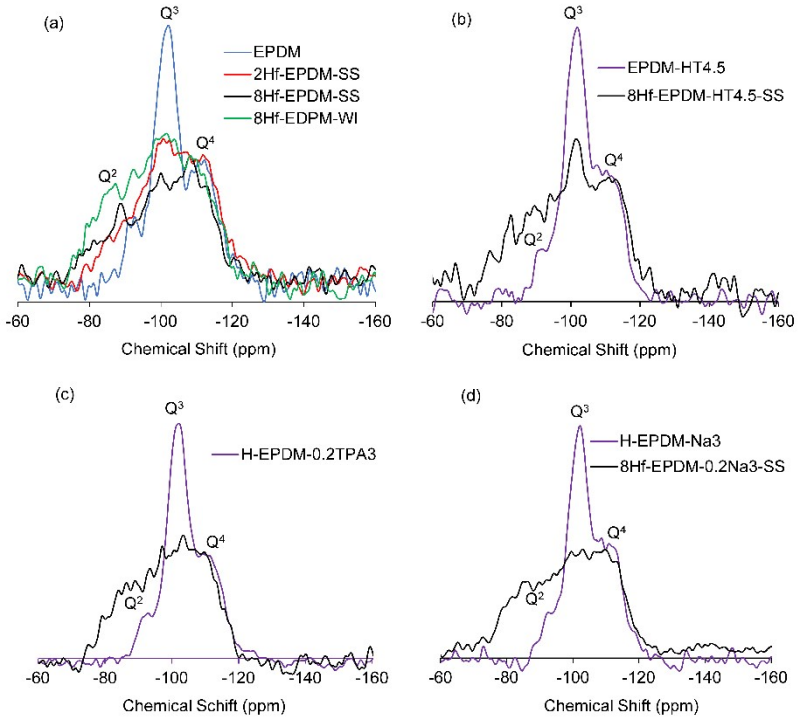

Figure S11. ^{29}Si{^{1}H} CP MAS NMR spectra of the EPDM silica supports and selected counterparts possessing a Hf loading of 2 wt% (2Hf) or 8 wt% (8Hf), prepared via the solid (SS) or wet (WI) impregnation method.

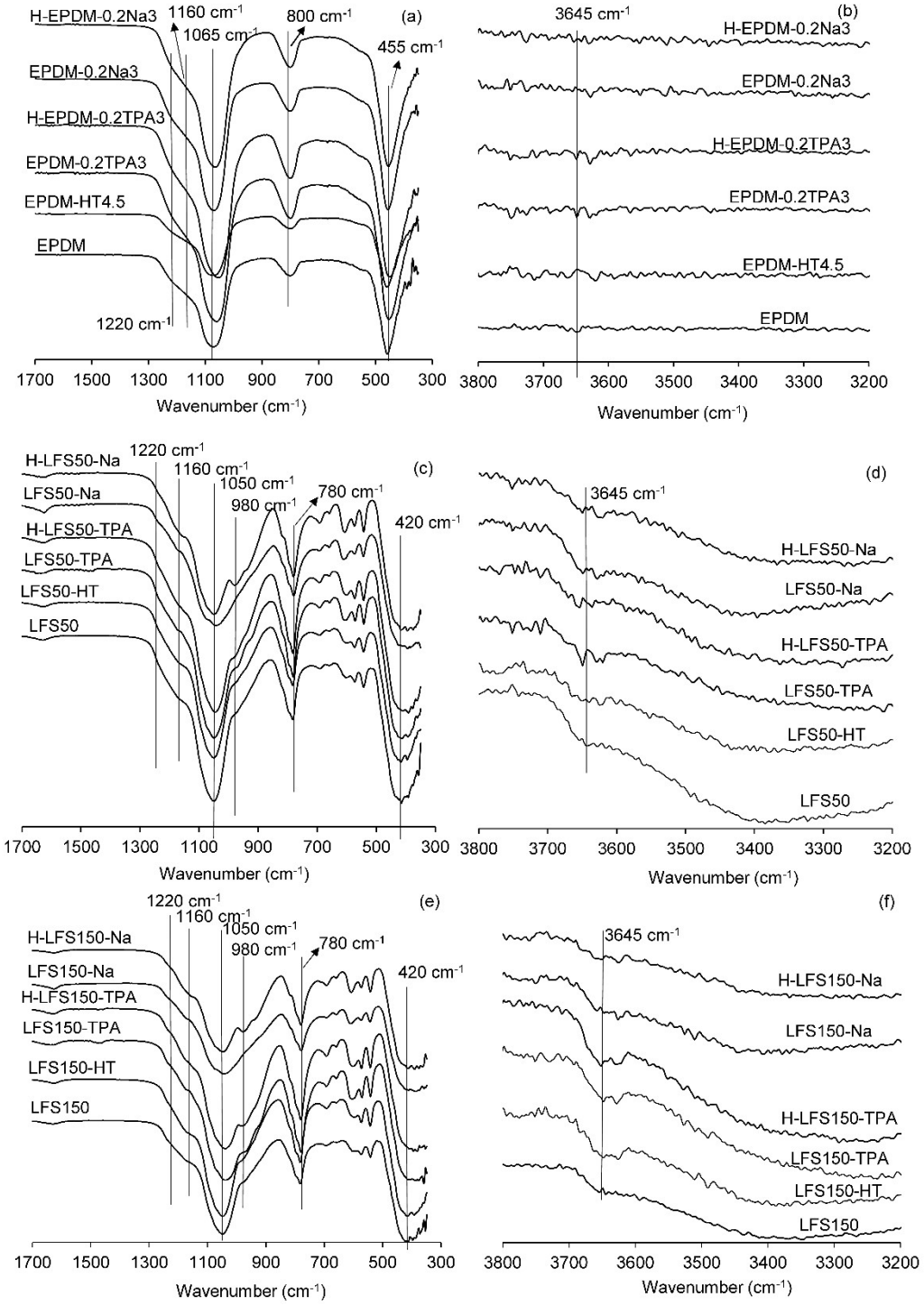

Figure S12. ATR FT-IR spectra of untreated and treated EPDM (a and b), untreated and treated LFS50 (c, d), and untreated and treated LFS150 (e, f). The lines serve as visual guides. The spectra in the range 3200-3800 cm^{-1} were enlarged 5x to facilitate the visualisation. The bands assignments are given in Table S3, based on literature data.

Table S3. ATR-FTIR spectral absorption bands for the untreated and treated EPDM, LFS50 and LFS150 silica supports, and possible assignments based on literature data.[2–5 a]

Sample	SiOH	Si-O-Si	Si-O-Si	Si-O-Si	Si-O-Si	Vicinal H-

	(Si-O stretch.	(Si–O bending)	Si–O Stretch (Internal Symm.)	stretch. (Internal Asymm.)	stretch. (External Asymm.)	bonded SiOH groups (OH vibrations
EPDM	-	459	800	1070	1220	-
EPDM-HT4.5	-	459	799	1071	1220	-
EPDM-0.2TPA3	-	453	799	1059	1220	-
H-EPDM-0.2TPA3	-	449	799	1053	1220	-
EPDM-0.2Na3	-	455	800	1069	1220	-
H-EPDM-0.2Na3	-	453	800	1065	1220	-
LFS50	~985	422	783	1049	1220	3651 3643 3633
LFS50-HT	~980	424	783	1047	1220	3658 3645 3620
LFS50-TPA	~975	422	781	1049	1220	3653 3634 3624
H-LFS50-TPA	~980	407	781	1044	1220	3647 3630
LFS50-Na	~980	422	779	1043	1220	3651 3642 2622
H-LFS50-Na	980	419	779	1047	1220	3645 3622
LFS150	~975	422	781	1049	1220	3648 3639 3630
LFS150-HT	~995	415	783	1047	1220	3659 3644 3617
LFS150-TPA	~980	413	779	1038	1220	3635 3611
H-LFS150-TPA	982	409	781	1040	1220	3645 3638 3611
LFS150-Na	~980	411	779	1043	1220	3653 3644 3613
H-LFS150-Na	978	415	781	1047	1220	3655 3644 3615

[a] Stretch = stretching; Symm = symmetric; Assym. = assymmetric.

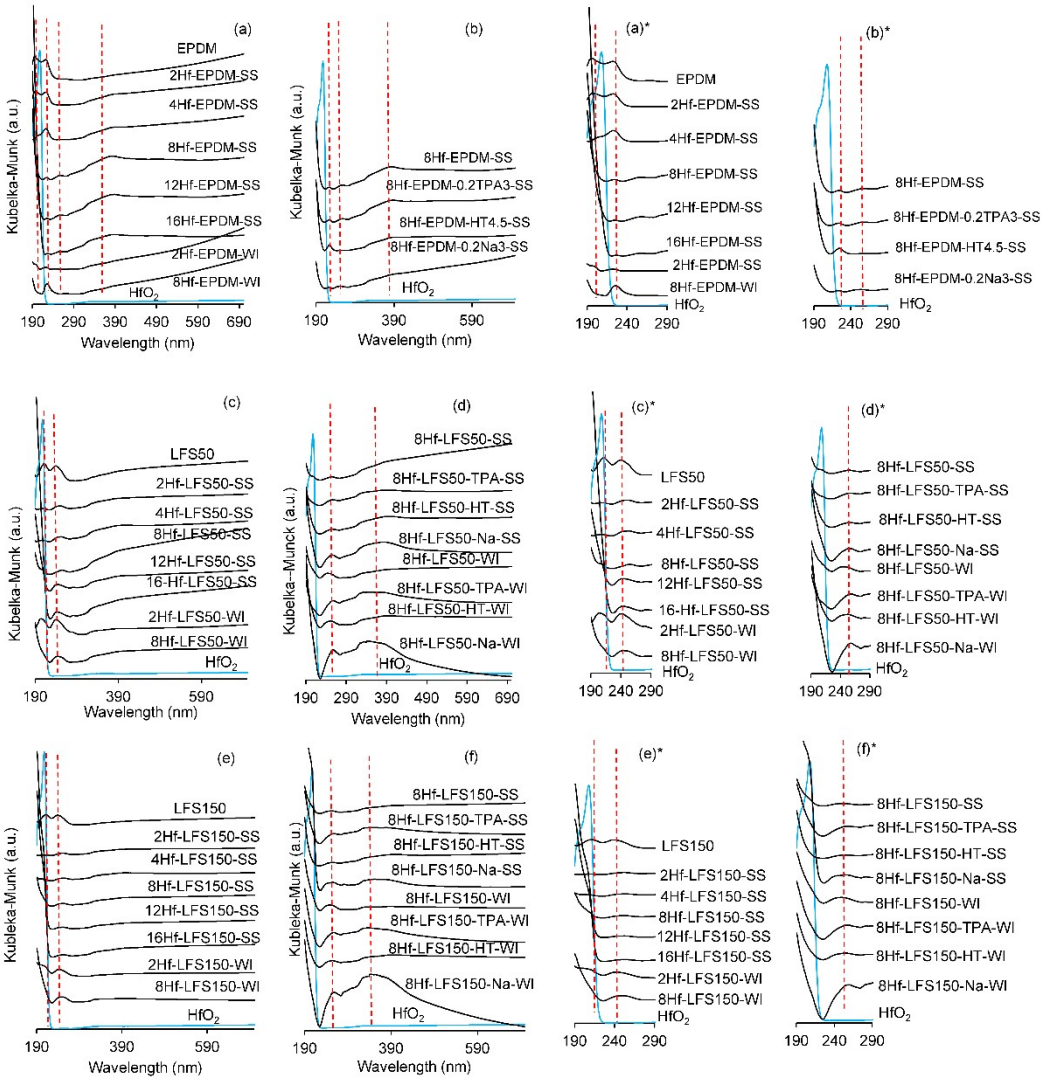

Figure S13. DR UV-Vis of untreated/treated EPDMs (a, b, a*, b*), untreated/treated LFS50s (c, d, c*, d*), and untreated/treated LFS150s (e, f, e*, f*). The vertical dashed lines mark band positions. The wavelength region of 190-290 nm was enlarged to facilitate visualisation.

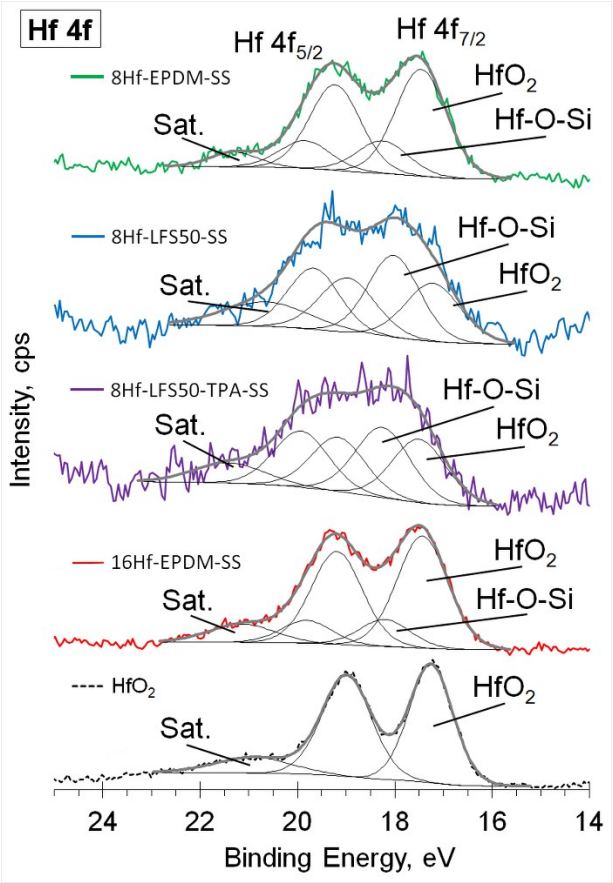

Figure S14. XPS fitted spectra in the Hf 4f region for 8Hf-EPDM-SS, 8Hf-LFS50-SS, 8Hf-LFS50-TPA-SS and 16Hf-EPDM-SS. The fitted spectrum of HfO_2 is included for comparison. Sat. = satellite peak, which may be due to differential charging effect in the XPS measurements.

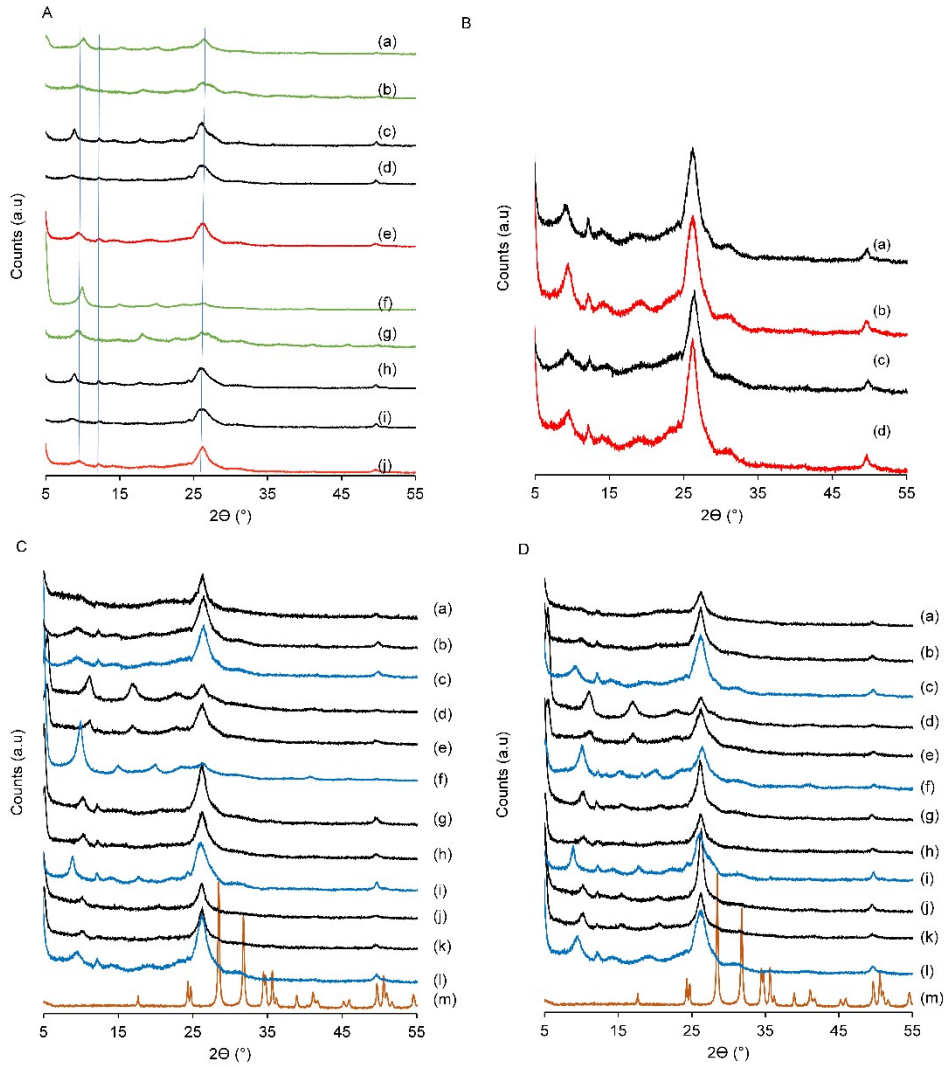

Figure S15. (A, B) PXRD patterns of untreated/treated LFS silica supports: **(A)** H-LFS150-Na (a); LFS150-Na (b); H-LFS150-TPA (c); LFS150-TPA (d); LFS150 (e); H-LFS50-Na (f); LFS50-Na (g); H-LFS50-TPA (h); LFS50-TPA (i); LFS50 (j); **(B)** LFS150-HT (a); LFS150 (b); LFS50-HT (c); LFS50. (C, D) PXRD patterns of the untreated/treated 2Hf-LFS50s or 2Hf-LFS150 and respective silica supports: **(C)** 2Hf-LFS50-HT (WI (a); SS (b)); LFS50-HT (c); 2Hf-LFS50-Na (WI (d); SS (e)); H-LFS50-Na (f); 2Hf-LFS50-TPA (WI (g); SS (h)); H-LFS50-TPA (i); 2Hf-LFS50 (WI (j); SS (k)); LFS50 (l); HfO_2 (m); **(D)** 2Hf-LFS150-HT (WI (a); SS (b)); LFS150-HT (c); 2Hf-LFS150-Na (WI (d); SS (e)); H-LFS150-Na (f); 2Hf-LFS150-TPA (WI (g); SS (h)); H-LFS150-TPA (i); 2Hf-LFS150 (WI (j); SS (k)); LFS150 (l); HfO_2 (m).

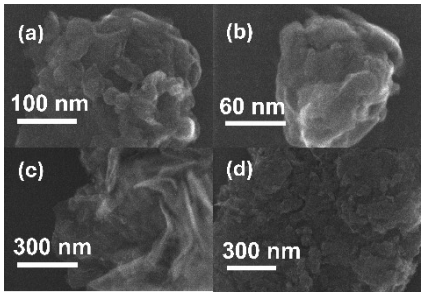

Figure S16. STEM images of LFS50 (a, b) and LFS150 (c, d).

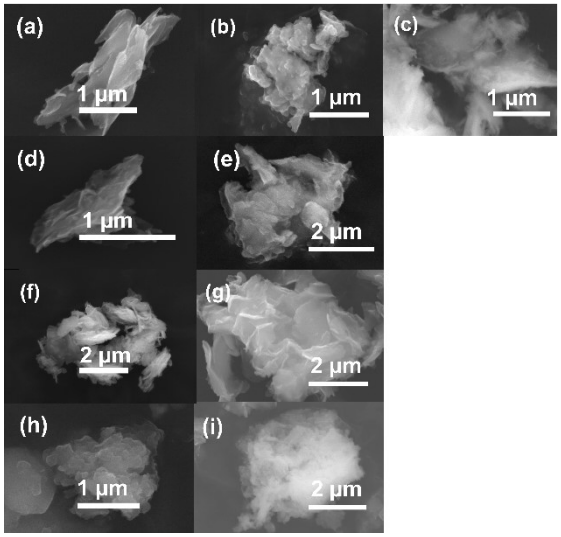

Figure S17. SEM images of (a) LFS50, (b) 8Hf-LFS50-S, (c) 8Hf-LFS50-WI, (d) LFS50-HT (e) 8Hf-LFS50-HT-WI, (f) H-LFS50-TPA, (g) 8Hf-LFS50-TPA-WI, (h) H-LFS50-Na, (i) 8Hf-LFS50-Na-WI.

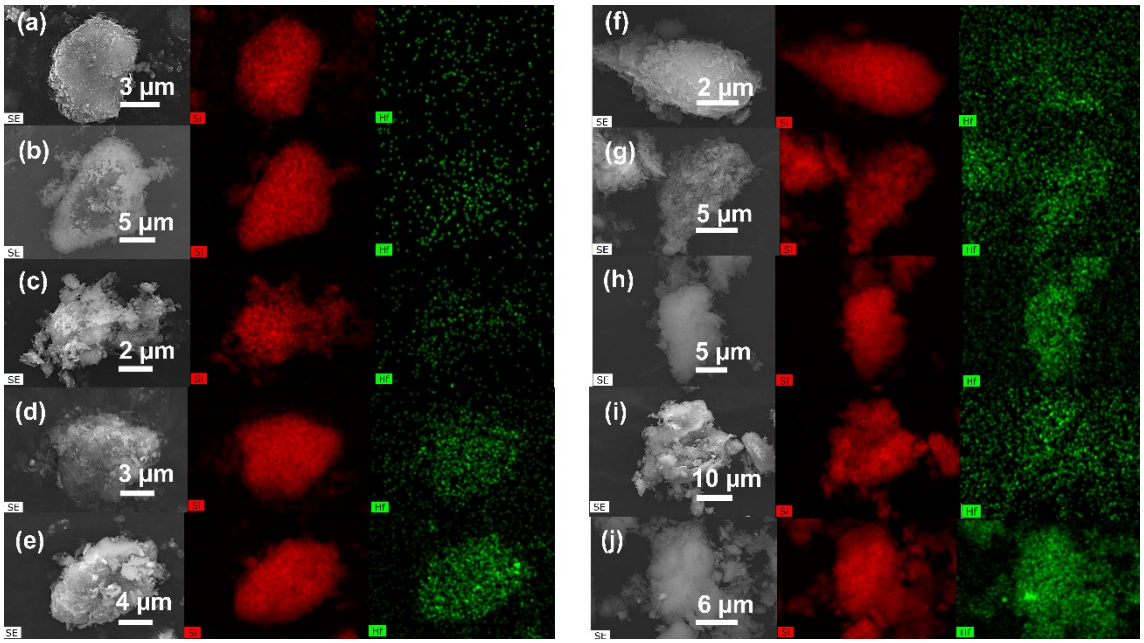

Figure S18. Elemental mappings of Si (red) and Hf (green) for 2Hf-LFS50-SS (a), 4Hf-LFS50-SS (b), 8Hf-LFS50-SS (c), 12Hf-LFS50-SS (d), 16Hf-LFS50-SS (e), 2Hf-LFS150-SS (f), 4Hf-LFS150-SS (g), 8Hf-LFS150-SS (h), 12Hf-LFS150-SS (i),16Hf-LFS150-SS (j).

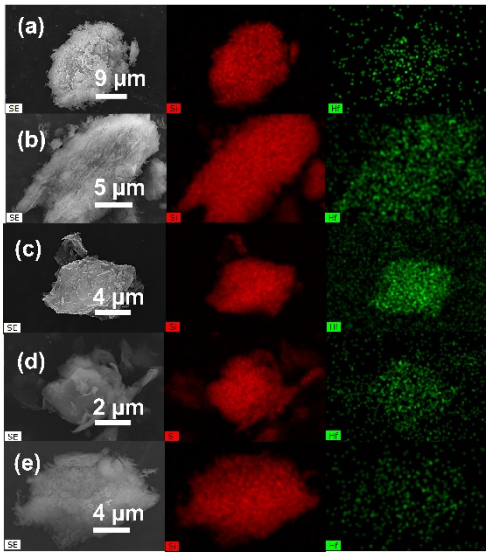

Figure S19. SEM images (a-e) and elemental mappings of Si (red) and Hf (green) for selected materials: 2Hf-LFS50-WI (a), 8Hf-LFS50-WI (b), 8Hf-LFS50-TPA-WI (c), 8Hf-LFS150-WI (d) and 8Hf-LFS150-TPA-WI (e).

Table S4. Elemental analysis and textural properties of the LFS50s.

Sample	Si/Hf (synth)[a]	Si/Hf (EDS)[a]	S_{BET} (m^2 g^{-1})	S_{meso} (m^2 g^{-1})	d_p (nm)
LFS50	-	-	218	149	2-10
2Hf-LFS50-SS	139	139	219	190	3-11
2Hf-LFS50-WI	139	128	222	156	2-11
4Hf-LFS50-SS	69	60	214	196	3-15
8Hf-LFS50-SS	35	43	194	127	2-10
8Hf-LFS50-WI	35	25	161	105	2-11
12Hf-LFS50-SS	23	22	-	-	-
16Hf-LFS50-SS	17	12	-	-	-
LFS50-HT	-	-	286	284	2-16
2Hf-LFS50-HT-SS	141	-	211	75	2-11
2Hf-LFS50-HT-WI	141	-	236	214	2-11
8Hf-LFS50-HT-SS	35	39	184	114	2-16
8Hf-LFS50-HT-WI	35	26	117	76	2-16
LFS50-TPA	-	-	179	163	2-10
H-LFS50-TPA	-	-	269	234	2-10
2Hf-LFS50-TPA-SS	137	-	263	250	2-9
2Hf-LFS50-TPA-WI	137	-	197	191	2-15
8Hf-LFS50-TPA-SS	34	38	175	165	2-10
8Hf-LFS50-TPA-WI	34	23	150	131	2-8
LFS50-Na	-	-	137	108	2-10
H-LFS50-Na	-	-	235	229	2-13
2Hf-LFS50-Na-SS	141	-	216	205	2-11
2Hf-LFS50-Na-WI	141	-	183	172	2-10
8Hf-LFS50-Na-SS	35	39	146	117	2-10
8Hf-LFS50-Na-WI	35	37	119	100	2-9

[a] Si/Hf molar ratio. Synth. = Si/Hf ratio based on the catalyst preparation conditions. EDS = Si/Hf ratio based on EDS measurements and considering the volatiles (water) content in the samples (measured by thermogravimetric analysis, TGA)). [b] S_{meso} was determined by the t-plot method (micropore volume was less than 0.04 cm^3 g^{-1} for the LFS50s).

Table S5. Elemental analysis and textural properties of the LFS150s.

Sample	Si/Hf (synth)[a]	Si/Hf (EDS)[a]	S_{BET} (m^2 g^{-1})	S_{meso} [b] (m^2 g^{-1})	d_p (nm)
LFS150	-	-	210	144	2-10
2Hf-LFS150-SS	143	142	204	186	2-11
2Hf-LFS150-WI	143	135	189	158	2-11
4Hf-LFS150-SS	71	75	-	-	-
8Hf-LFS150-SS	36	38	202	137	2-16
8Hf-LFS150-WI	36	33	165	110	2-11
12Hf-LFS150-SS	24	22	-	-	-
16Hf-LFS150-SS	18	12	-	-	-
LFS150-HT	-	-	251	162	3-11
2Hf-LFS150-HT-SS	139	-	225	144	2-15
2Hf-LFS150-HT-WI	139	-	182	140	2-15
8Hf-LFS150-HT-SS	35	27	200	181	2-10
8Hf-LFS150-HT-WI	35	24	145	87	2-10
LFS150-TPA	-	-	168	119	3-14
H-LFS150-TPA	-	-	215	164	1-10
2Hf-LFS150-TPA-SS	136	-	193	127	1-10
2Hf-LFS150-TPA-WI	136	-	184	144	2-11
8Hf-LFS150-TPA-SS	34	38	170	109	2-9
8Hf-LFS150-TPA-WI	34	35	181	184	2-12
LFS150-Na	-	-	139	121	3-11
H-LFS150-Na	-	-	249	200	2-10
2Hf-LFS150-Na-SS	140	-	213	193	3-18
2Hf-LFS150-Na-WI	140	-	174	152	2-18
8Hf-LFS150-Na-SS	35	30	186	138	2-20
8Hf-LFS150-Na-WI	35	33	186	140	2-10

[a] Si/Hf molar ratio. Synth. = Si/Hf ratio based on the catalyst preparation conditions. EDS = Si/Hf ratio based on EDS measurements and considering the volatiles (water) content in the samples (measured by thermogravimetric analysis, TGA)). [b] S_{meso} was determined by the t-plot method (micropore volume was less than 0.04 cm^3 g^{-1} for the LFS150s).

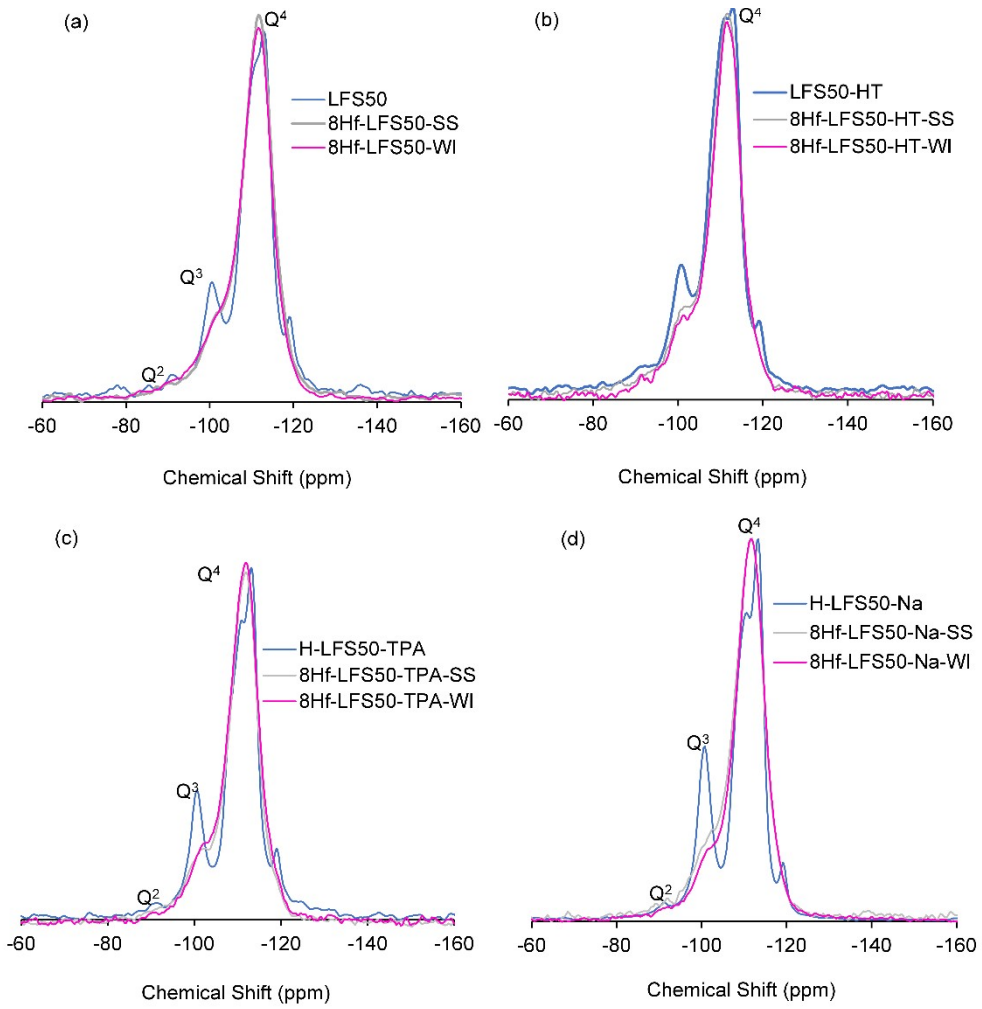

Figure S20. ^{29}Si MAS NMR spectra of untreated/treated LFS50 before and after Hf impregnation via different methods (f-i).

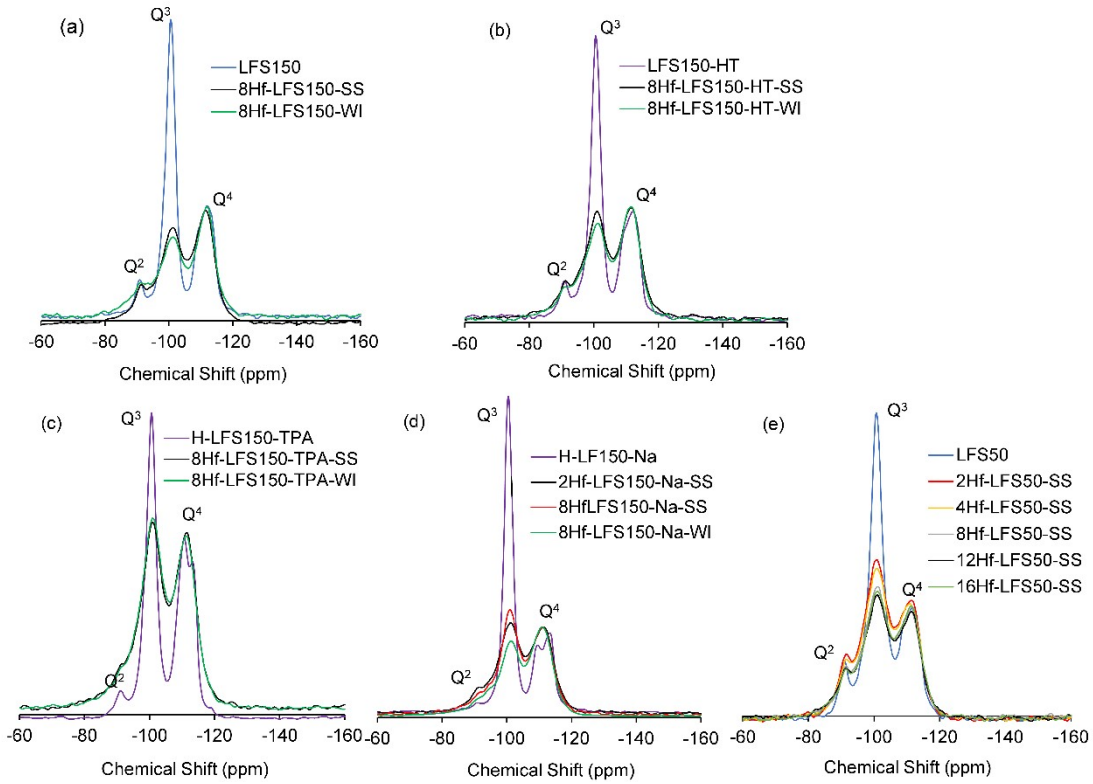

Figure S21. $^{29}Si\{^{1}H\}$ CP MAS NMR spectra (a-d) of different LFS150 silica supports and selected counterparts possessing a Hf loading of 2 wt% (Hf) or 8 wt% (Hf), prepared via solid state (SS) or wet (WI) impregnation method; and $^{29}Si\{^{1}H\}$ CP MAS NMR spectra (e) of untreated LFS50 before and after impregnation of different Hf loadings via the S method.

D. CATALYTIC STUDIES

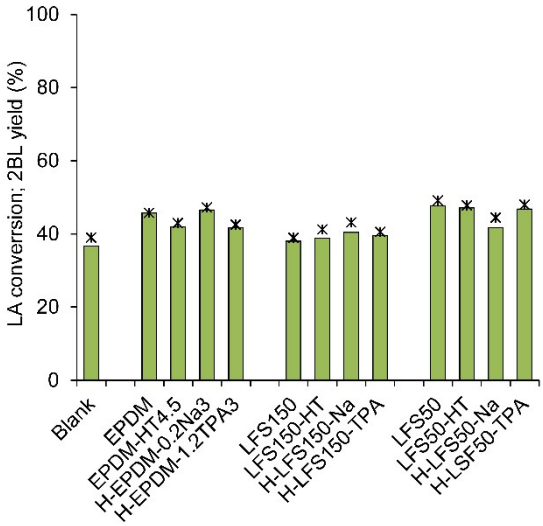

Figure S22. LA conversion (*) to 2 BL (green bars) at 24 h, without catalyst (blank) or in the presence of the silica supports without Hf. Reaction conditions: 0.45 M LA in 2BuOH, 25.5 g_{cat} L^{-1}, 180 °C.

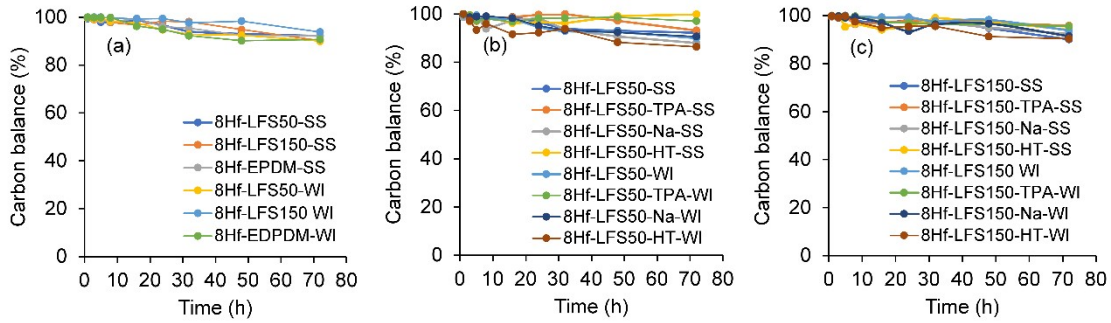

Figure S23. Carbon balances for the untreated (a) and treated LFS50s (b) and LFS150s (c).

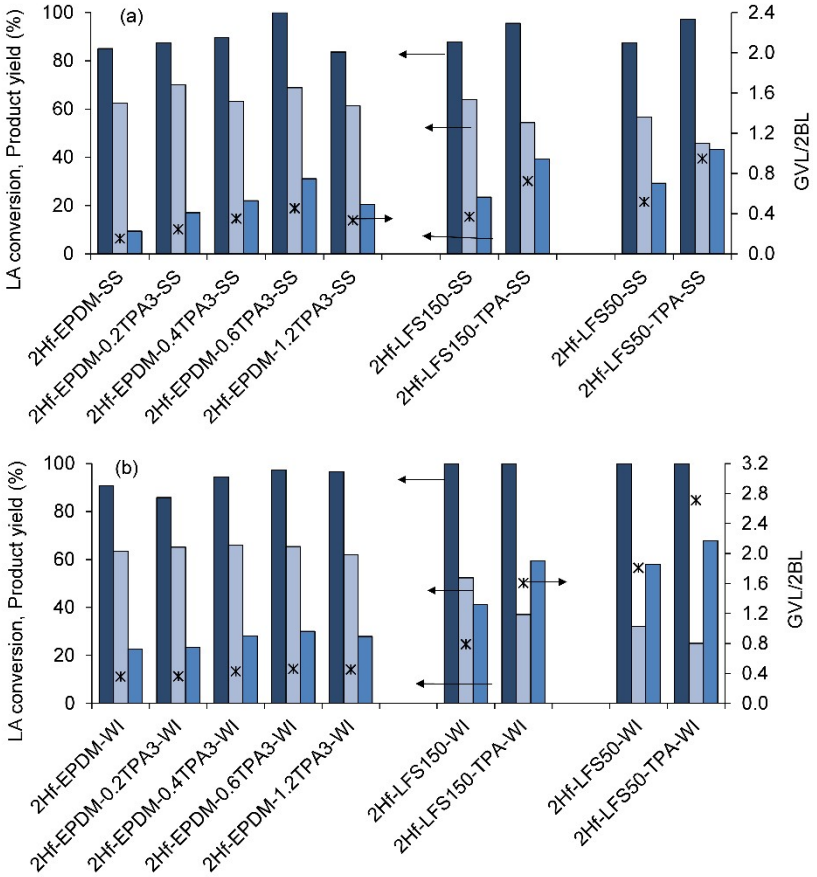

Figure S24. Influence of the TPAOH concentration and impregnation method (SS (a, c) or WI (b, d) method), on the performances of the 2Hf-silicas. LA conversion (dark blue bars) to 2BL (light blue bars) and GVL (blue bars) at 48 h; (*) is the GVL/2BL molar ratio. Reaction conditions: 0.45 M LA in 2BuOH, 25.5 g_{cat} L^{-1}, 180 °C.

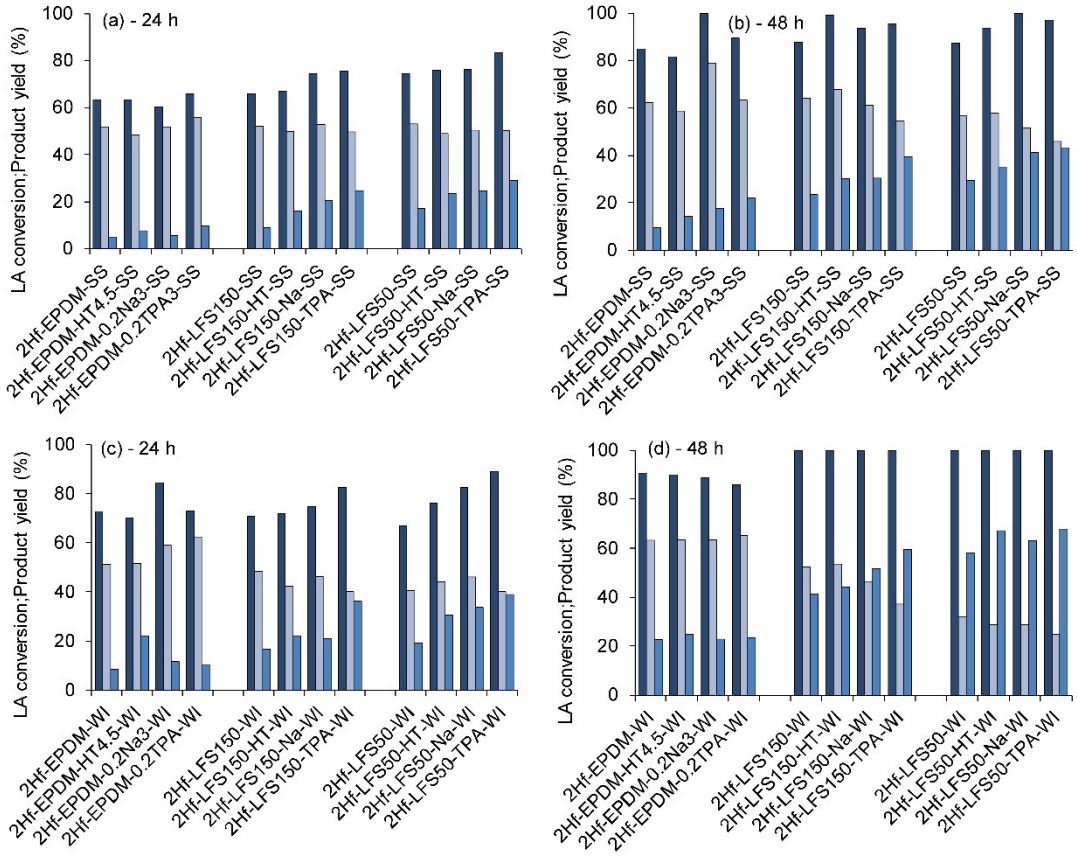

Figure S25. Influence of the type of treatment (HT, Na, TPA) of the supports and impregnation method (SS (a, b) or WI (c, d) method), on the performances of the 2Hf-silicas. LA conversion (dark blue bars) to 2BL (light blue bars) and GVL (blue bars) at 24 h (a, c) or 48 h (b, d). Reaction conditions: 0.45 M LA in 2BuOH, 25.5 g_{cat} L^{-1}, 180 °C.

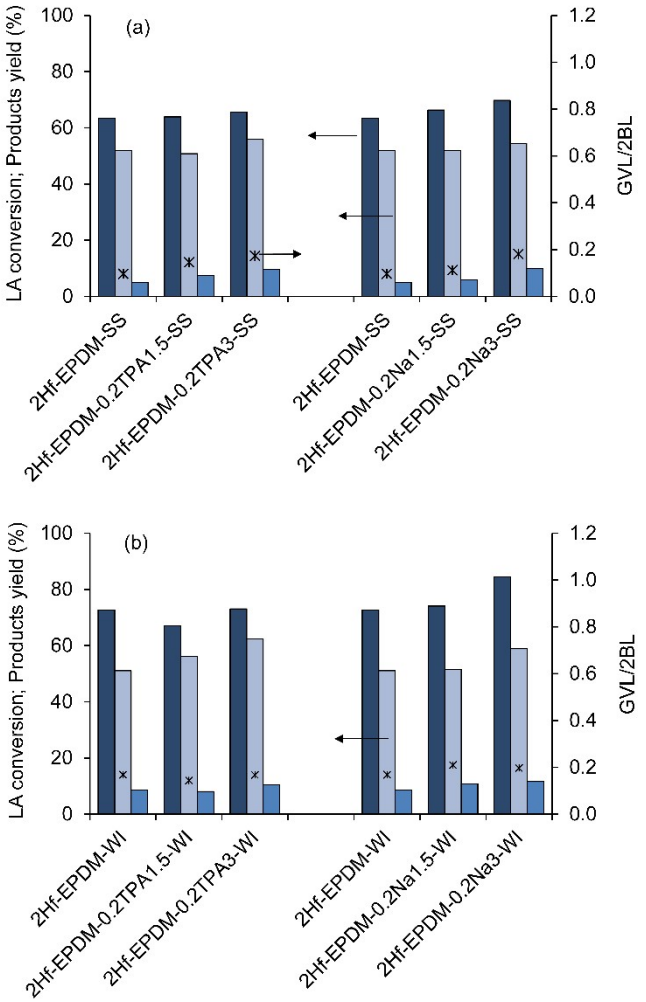

Figure S26. Influence of the alkaline treatment time (t= 1.5 h or 3 h) on the performances of the 2Hf-EPDMs, prepared via the SS (a) or WI (b) impregnation method. LA conversion (dark blue bars) to 2BL (light blue bars) and GVL (blue bars), at 24 h; (*) is the GVL/2BL molar ratio. Reaction conditions: 0.45 M LA in 2BuOH, 25.5 g_{cat} L^{-1}, 180 °C.

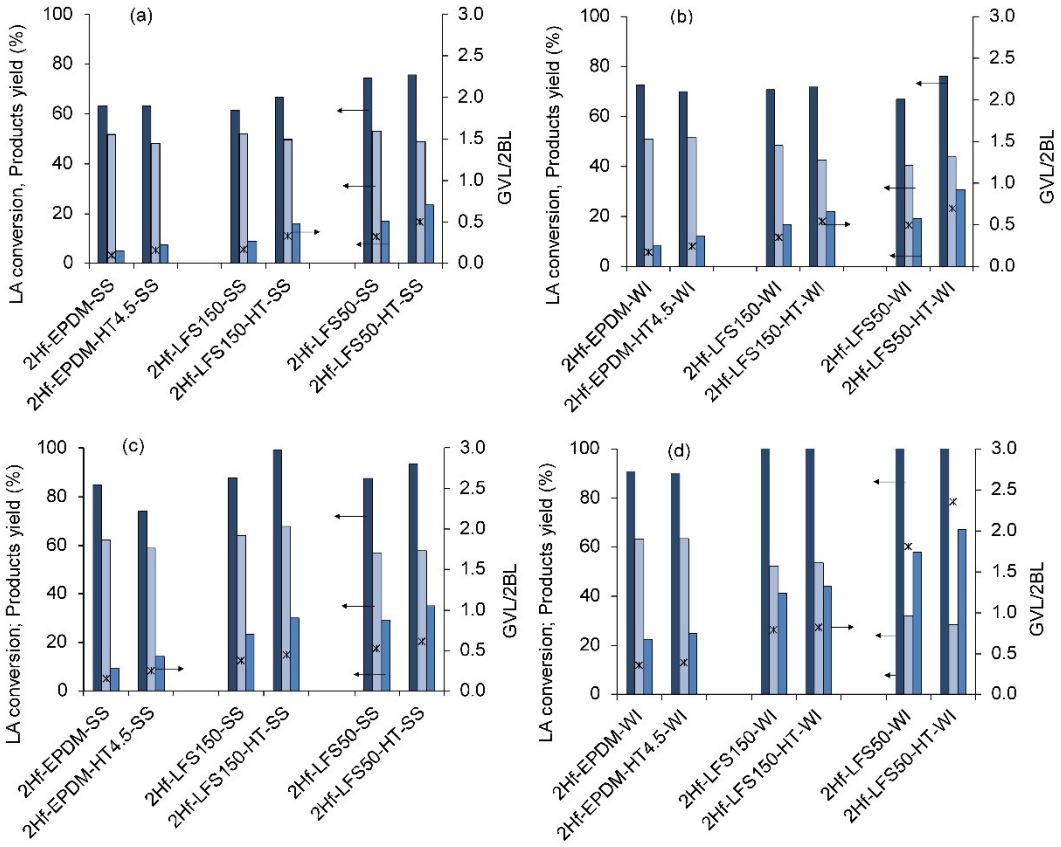

Figure S27. Influence of the HT-treatment and type of impregnation method (SS (a, c) or WI (b, d) method) on the catalytic performances of the 2Hf-silicas for the LA conversion (dark blue bars) to 2BL (light blue bars) and GVL (blue bars), and GVL/2BL molar ratio (*), at 24 h (a, b) or 48 h (c, d). Reaction conditions: 0.45 M LA in 2BuOH, 25.5 g_{cat} L^{-1}, 180 °C.

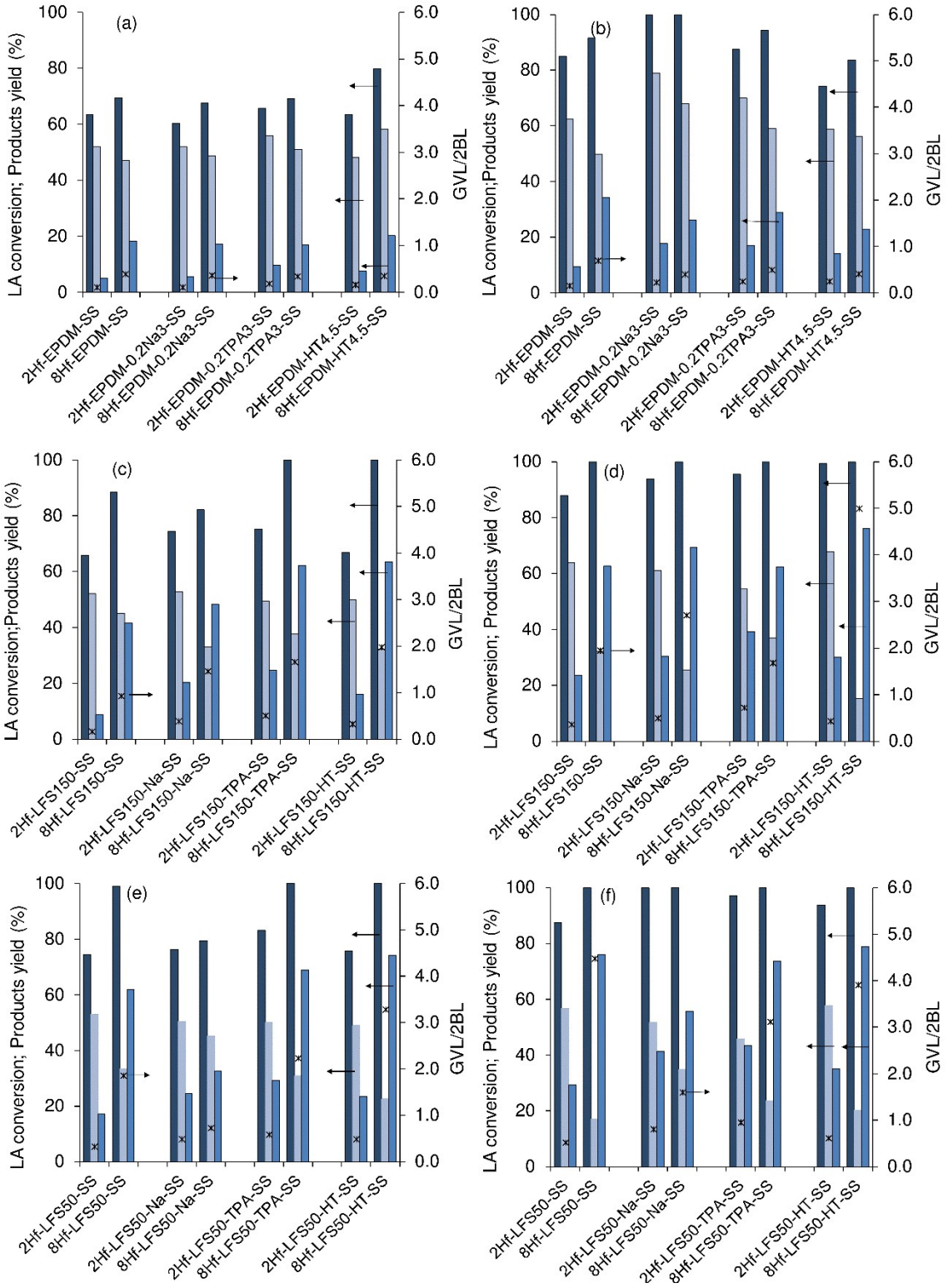

Figure S28. Comparison of the LA conversion (blue bars) to 2BL (green bars) and GVL (red bars) at 24 h (a, c, e) or 48 h (b, d, f), for 2 wt% Hf and 8 wt% Hf loading (SS method) on EPDM (a, d), LFS150 (b, e) and LFS50 (c, f); (*) is the GVL/2BL molar ratio. Reaction conditions: 0.45 M LA in 2BuOH, 25.5 g_{cat} L^{-1}, 180 °C.

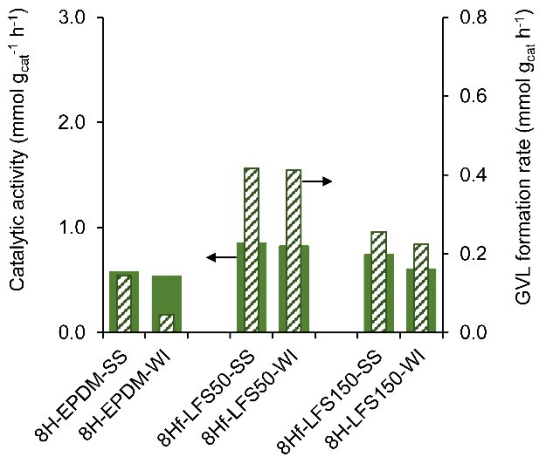

Figure S29. Catalytic activity and GVL formation rate for the untreated 8Hf-silicas prepared via the SS or WI impregnation method. Reaction conditions: 0.45 M LA in 2BuOH, 25.5 g_{cat} L^{-1}, 16 h, 180 °C.

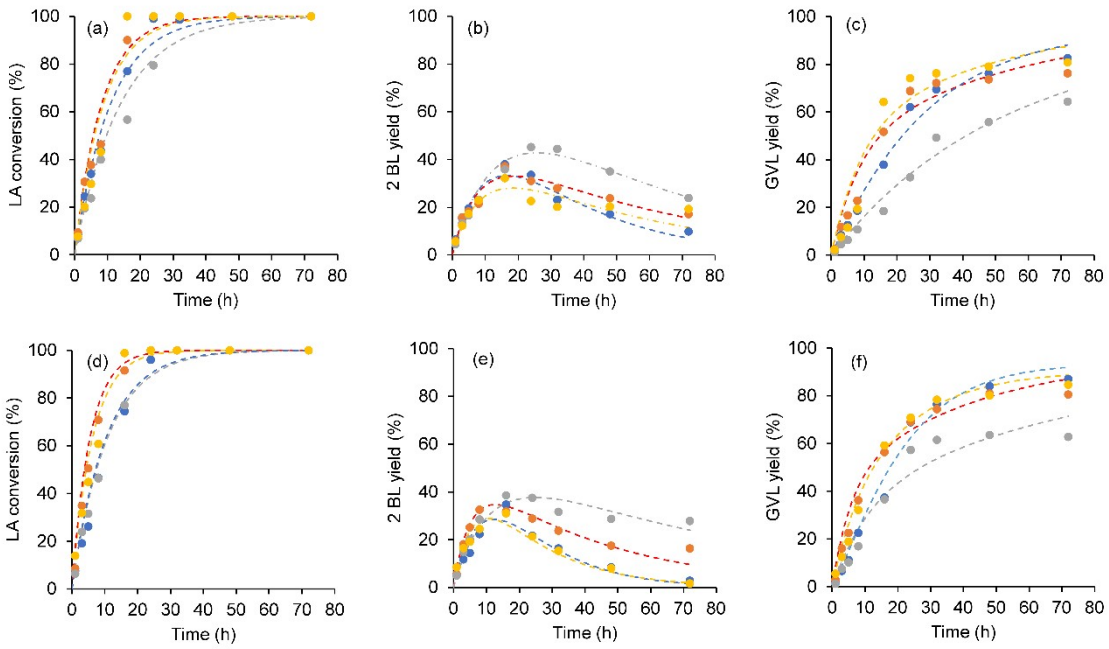

Figure S30. Kinetic model fitting (dashed lines) to the experimental data (points) for the LA conversion (a, d), 2BL yield (b, e) and GVL yield (c, f) versus time, for the untreated/treated 8Hf-LFS50s, prepared via the SS (a-c) or WI (d-f) impregnation method. Specifically, untreated 8Hf-LFS50s – blue; and treated 8Hf-LFS50-TPA materials – orange, 8Hf-LFS50-HT materials – yellow, and 8Hf-LFS50-Na materials - grey. Reaction conditions: 0.45 M LA in 2BuOH, 25.5 g_{cat} L^{-1}, 180 °C.

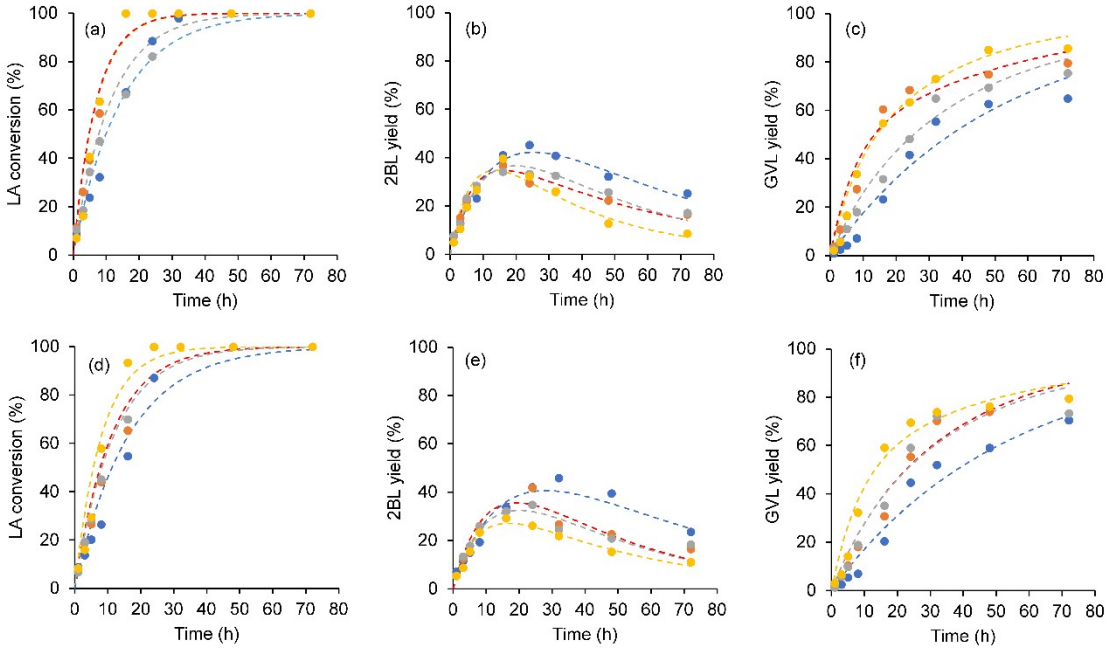

Figure S31. Kinetic model fitting (dashed lines) to the experimental data (points) for the LA conversion (a, d), 2BL yield (b, e) and GVL yield (c, f) versus time for the 8Hf-LFS150s, prepared via the SS (a-c) or WI (d-f) impregnation method. Specifically, untreated 8Hf-LFS150- blue; and treated 8Hf-LFS150-TPA materials – orange, 8Hf-LFS150-HT materials – yellow, and 8Hf-LFS150-Na materials - grey. Reaction conditions: 0.45 M LA in 2BuOH, 25.5 g_{cat} L^{-1}, 180 °C.

Table S6. Kinetic constants (k_i; L g_{cat}^{-1} h^{-1}) on the conversion of LA to GVL, in the presence of Hf-silicas

Catalyst	Kinetic constants (k_i) (Reaction steps)				
	k_1 (LA to 2BL)	**k_2 (2BL to GVL)**	**k_3 (LA to GVL)**	**k_4 (LA decomposition)**	**F_{obj}**
8Hf-EPDM-SS	1.58×10^{-3}	4.45×10^{-4}	2.69×10^{-4}	1.21×10^{-4}	1.10×10^{-3}
8Hf-EPDM-WI	1.64×10^{-3}	4.68×10^{-4}	1.09×10^{-4}	1.01×10^{-4}	1.08×10^{-2}
8Hf-LFS50-SS	2.20×10^{-3}	1.45×10^{-3}	1.20×10^{-3}	1.72×10^{-4}	8.40×10^{-3}
8Hf-LFS50-WI	2.44×10^{-3}	2.57×10^{-3}	1.10×10^{-3}	2.42×10^{-4}	8.70×10^{-3}
8Hf-LFS150-SS	1.89×10^{-3}	7.61×10^{-4}	7.61×10^{-4}	8.19×10^{-5}	8.40×10^{-3}
8Hf-LFS150-WI	1.62×10^{-3}	7.06×10^{-4}	7.37×10^{-4}	3.90×10^{-5}	1.89×10^{-2}
8Hf-LFS50-TPA-SS	2.17×10^{-3}	6.67×10^{-4}	2.52×10^{-3}	7.02×10^{-5}	1.54×10^{-2}
8Hf-LFS50-TPA-WI	3.37×10^{-3}	9.36×10^{-4}	3.53×10^{-3}	2.34×10^{-4}	6.50×10^{-3}
8Hf-LFS50-Na-SS	1.91×10^{-3}	7.10×10^{-4}	7.06×10^{-4}	1.83×10^{-4}	9.60×10^{-3}
8Hf-LFS50-Na-WI	1.87×10^{-3}	4.95×10^{-4}	1.58×10^{-3}	1.64×10^{-4}	1.33×10^{-2}
8Hf-LFS50-HT-SS	1.82×10^{-3}	7.84×10^{-4}	2.62×10^{-3}	3.90×10^{-5}	2.93×10^{-2}
8Hf-LFS50-HT-WI	3.07×10^{-3}	1.95×10^{-3}	2.59×10^{-3}	5.89×10^{-4}	1.13×10^{-2}
8Hf-LFS150-TPA-SS	2.64×10^{-3}	7.25×10^{-4}	2.89×10^{-3}	9.36×10^{-5}	1.35×10^{-2}
8Hf-LFS150-TPA-WI	2.10×10^{-3}	1.05×10^{-3}	1.34×10^{-3}	7.32×10^{-5}	1.44×10^{-2}
8Hf-LFS150-Na-SS	2.08×10^{-3}	9.52×10^{-4}	1.26×10^{-3}	1.60×10^{-4}	1.05×10^{-2}
8Hf-LFS150-Na-WI	1.82×10^{-3}	1.03×10^{-3}	1.35×10^{-3}	1.29×10^{-4}	1.59×10^{-2}
8Hf-LFS150-HT-SS	2.96×10^{-3}	1.23×10^{-3}	2.47×10^{-3}	1.29×10^{-4}	9.60×10^{-3}
8Hf-LFS150-HT-WI	1.91×10^{-3}	8.89×10^{-4}	2.67×10^{-3}	2.34×10^{-4}	1.21×10^{-2}

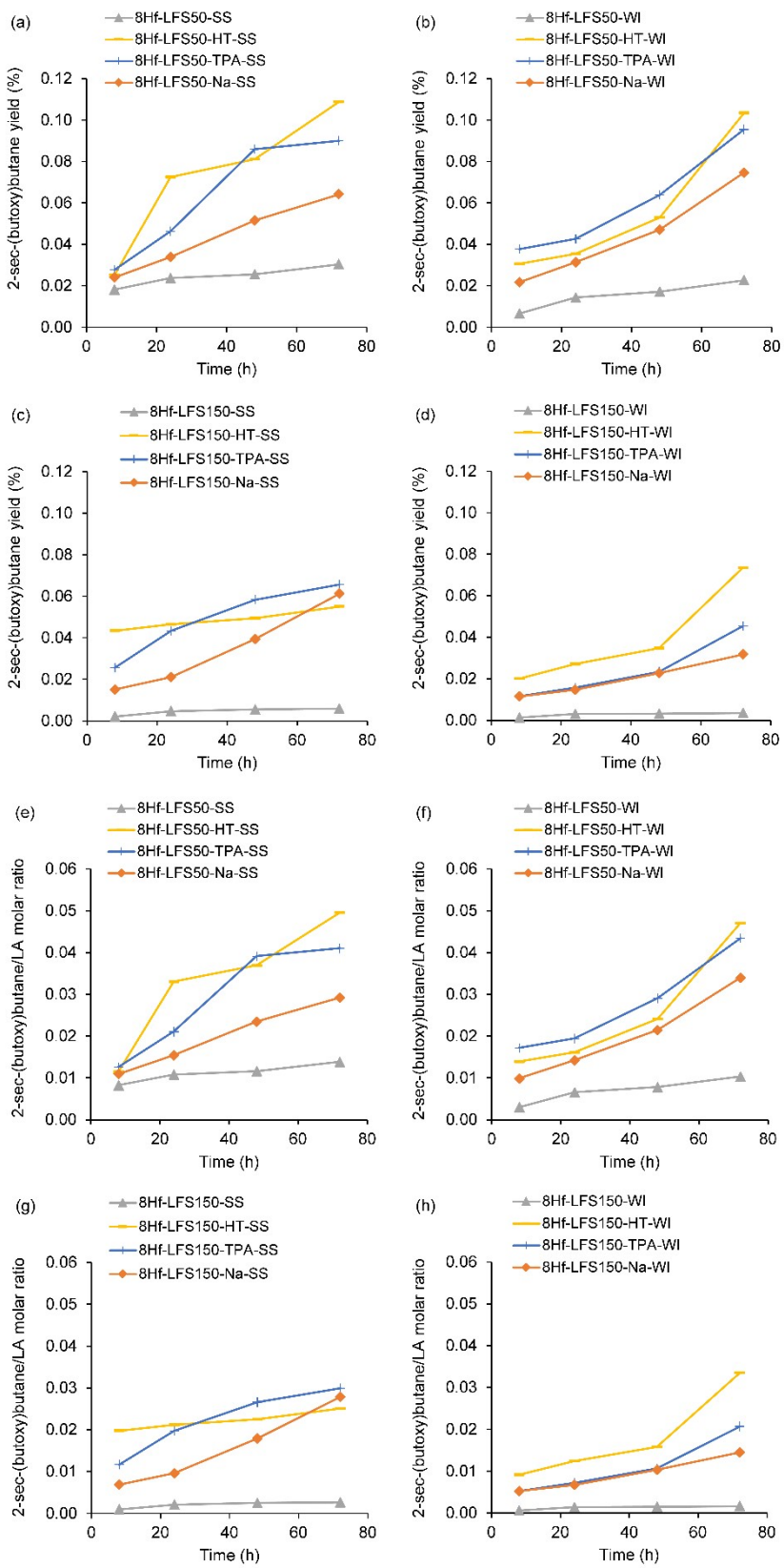

Figure S32. Kinetic profiles of formation of 2-sec-(butoxy)butane (expressed as yield based on the initial moles of 2BuOH (a-d), or expressed as molar ratio of 2-sec-(butoxy)butane/(initial moles of LA) (e-h)) via 2BuOH decomposition, in the presence of the 8Hf-LFSs. Reaction conditions: 0.45 M LA in 2BuOH, 25.5 g_{cat} L^{-1}, 180 °C.

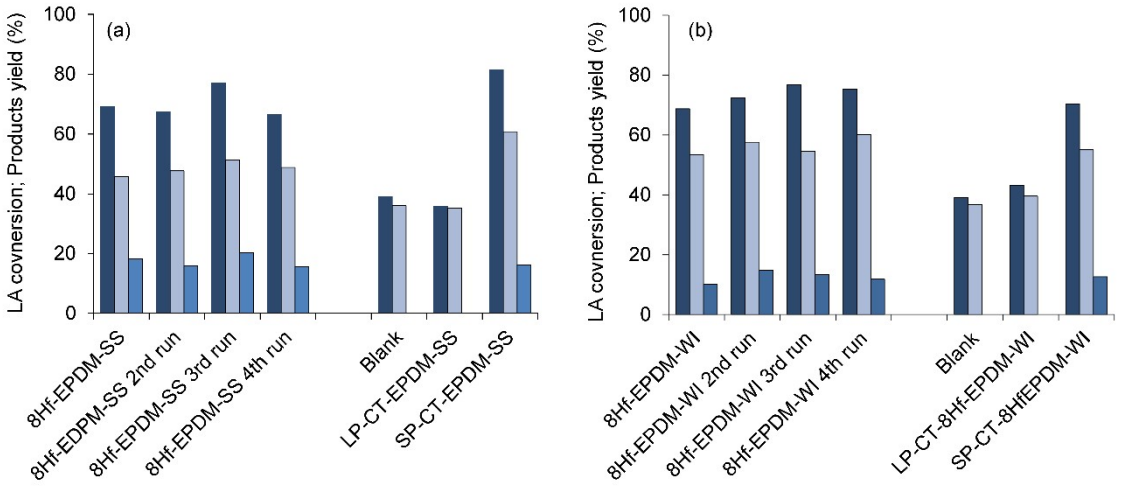

Figure S33. Catalytic stability of 8Hf-EPDM-SS (a) and 8Hf-EPDM-WI (b) in the conversion of LA (blue bars) to 2BL (green bars) and GVL (red bars) at 180 °C at 24 h. The results without catalyst and the liquid and solid phases of the contact tests (LP-CT-EPDM-SS and SP-CT-EPDM-WI) are given for comparison. Reaction conditions: 0.45 M LA in 2BuOH, 25.5 g_{cat} L^{-1}, 180 °C.

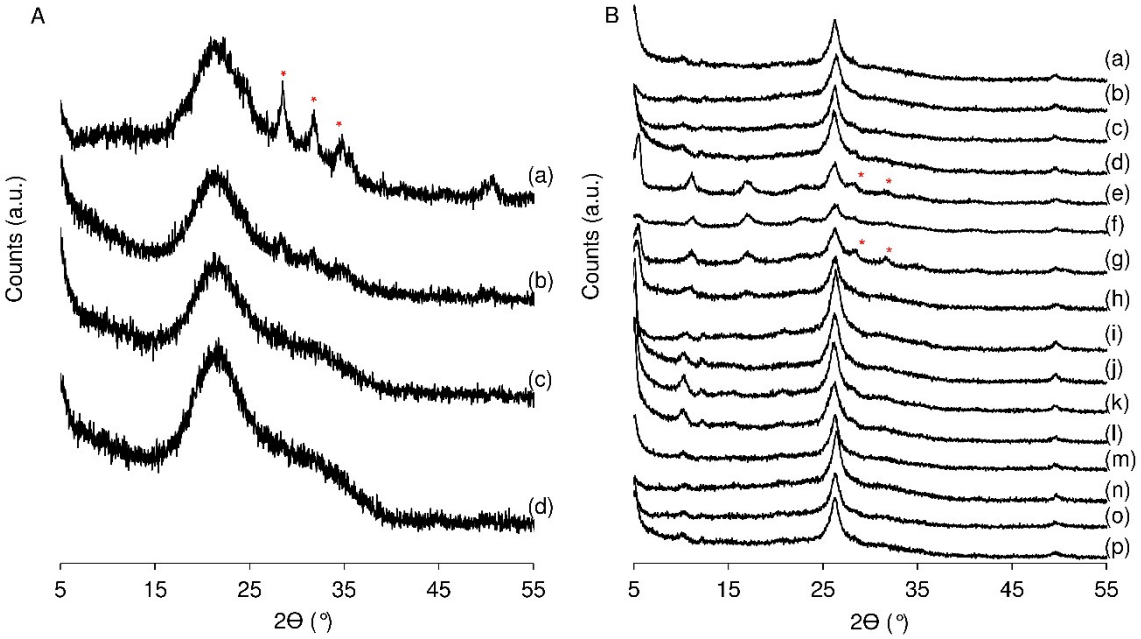

Figure S34. PXRD patterns of the used versus original catalysts: **(A)** 8Hf-EPDM-WI used (a), 8Hf-EPDM-WI (b), 8Hf-EPDM-SS used (c), and 8Hf-EPDM-SS (d); **(B)** 8Hf-LFS50-HT-WI used (a), 8Hf-LFS50-HT-WI (b), 8Hf-LFS50-HT-SS used (c), 8Hf-LFS50-HT-SS (d), 8Hf-LFS50-Na-WI used (e), 8Hf-LFS50-Na-WI (f), 8Hf-LFS50-Na-SS used (g), 8Hf-LFS50-Na-SS (h), 8Hf-LFS50-TPA-WI used (i), 8Hf-LFS50-TPA-WI (j), 8Hf-LFS50-TPA-SS used (k), 8Hf-LFS50-TPA-SS (l), 8Hf-LFS50-WI used (m), 8Hf-LFS50-WI (n), 8Hf-LFS50-SS used (o), and 8Hf-LFS50-SS (p). The red asterisks signalise peaks associated with HfO_2.

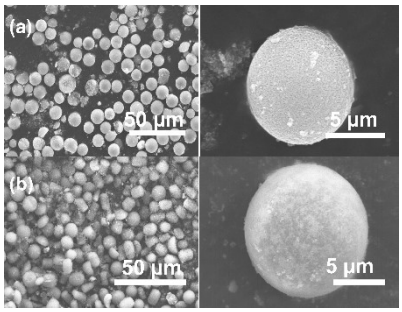

Figure S35. SEM images at different magnifications of original 8Hf-EPDM-WI (a) and used 8Hf-EPDM-WI (b).

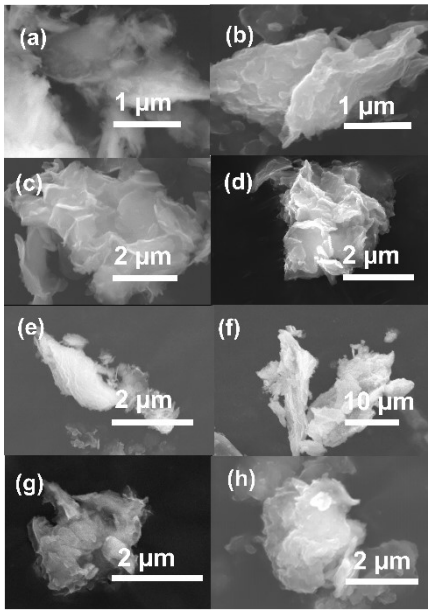

Figure S36. SEM images of 8Hf-LFS50-WI (a); 8Hf-LFS50-WI used (b); 8Hf-LFS50-TPA-WI (c); 8Hf-LFS50-TPA-WI used (d); 8Hf-LFS50-Na-WI (e), 8Hf-LFS50-Na-WI used (f), 8Hf-LFS50-HT-WI (g) and 8Hf-LFS50-HT-WI used (h).

Table S7. The molar ratio Si/Hf of the original and used catalysts.[a]

Catalyst	Si/Hf (fresh catalyst)	Si/Hf (used)
8Hf-EPDM-SS	34	39
8Hf-EPDM-WI	40	37
8Hf-LFS50-SS	43	38
8Hf-LFS50-WI	25	27
8Hf-LFS50-TPA-SS	38	38
8Hf-LFS50-TPA-WI	23	23
8Hf-LFS50-Na-SS	39	39
8Hf-LFS50-Na-WI	37	45
8Hf-LFS50-HT-SS	39	39
8Hf-LFS50-HT-WI	24	26

[a] Measured by EDS.

Table S8. Fully inorganic transition metal/silica catalysts reported in the literature for the CTH of LA to GVL, in alcohol media.[6–14]

	Catalyst	H-donor	T [a] (°C)	$[LA]_0$ [a] (M)	LA/Cat [a] (m/m)	t [a] (h)	Conv. [a] (%)	GVL yield (%)	Stability in consecutive runs (unless otherwise mentioned) [a]	Ref.
1	8Hf-LFS50-SS	2BuOH	180	0.45	2.0	24	99	62	Stable for 4 runs	-
2	8Hf-LFS50-HT-SS	2BuOH	180	0.45	2.0	24	100	74	Stable for 4 runs	-
3	8Hf-LFS50-TPA-SS	2BuOH	180	0.45	2.0	24	100	69	Stable for 4 runs	-
4	8Hf-LFS50-WI	2BuOH	180	0.45	2.0	24	96	69	Stable for 4 runs	
5	8Hf-LFS50-HT-WI	2BuOH	180	0.45	2.0	24	100	71	Stable for 4 runs	
6	8Hf-LFS50-TPA-WI	2BuOH	180	0.45	2.0	24	100	69	Stable for 4 runs	
7	Hf-TUD-1(50) (Si/Hf = 50)	2BuOH	200	0.45	2.0	24	100	29	nm	8
8	ZrO_2-SBA-15 (10 wt% Zr)	2PrOH	150	0.2	5.8	3	99.5	91	GVL yield decreased	9
9	ZrO_2-SBA-15 (23 wt% Zr)[b]	2BuOH	250	1.57	nm	nm[c]	100	96	GVL decreased from 96 % to *ca*. 80 % along 20 h on-stream	10
10	ZrP/SBA-15 (15 wt% Zr)	2PrOH	180	0.17	2.0	2	96	52	LA conversion and GVL yield decreased slightly	15
11	Zr-SBA-15(2) (24 wt% Zr)[c]	2PrOH	190	0.16	1.5	1.5	100	94	nm	12
12	Zr-SBA-15(20) (Si/Zr = 20)	2BuOH	160	0.16	0.5	28	>99	95	Stable for 5 runs	13
13	SZ+ZrO_2-SBA-15[d]	2PrOH	150	0.13	5.8	0.83[e]	85	80	nm	6
14	SZ+ZrO_2-SBA-15mix[d,f]	2PrOH	150	0.13	11.6	6.5	89	32	nm	6
15	SnO_2/SBA-15 (Si/Sn = 53)	2PrOH	110	0.73	2.5	8	85	81	Stable for 6 runs	7
16	Sn-SBA-15	2PrOH	200	2.45	nm	3	72	71	nm	14
17	Zr-KIT-5(10)	2PrOH	180	0.20	1.16	6	97	89	Stable for 5 runs	16

[a] T = reaction temperature, $[LA]_0$ = initial LA concentration, LA/Cat = LA/catalyst mass ratio, t = reaction time, Conv. = LA conversion; nm = not mentioned. [b] Continuous operation mode, with liquid feed flow rate = 1 mL h^{-1}. [c] ZrO_2 on SBA-15 by co-precipitation and layer by layer deposition. [d] SZ = sulphated zirconia (continuous flow in dual bed reactor). [e] Residence time. [f] Mechanical mixture.

References

1 M. Colilla, M. Martínez-Carmona, S. Sánchez-Salcedo, M. L. Ruiz-González, J. M. González-Calbet and M. Vallet-Regí, J. Mater. Chem. B, 2014, 2, 5639–5651.
2 T. Karbowiak, M. A. Saada, S. Rigolet, A. Ballandras, G. Weber, I. Bezverkhyy, M. Soulard, J. Patarin and J. P. Bellat, Phys. Chem. Chem. Phys., 2010, 12, 11454–11466.
3 S. A. Kozlova and S. D. Kirik, Micropor. Mesopor. Mat., 2010, 133, 124–133.
4 K. F. M. G. J. Scholle, W. S. Veeman, P. Frenken and G. P. M. van der Velden, Appl. Catal., 1985, 17, 233–259.
5 S. M. Shawky, A. A. Abo-AlHassan, H. Lill, D. Bald, S. FEL-Khamisy and E.-Z. M. Ebeid, J Nanosci Curr Res, 2016, 1, 103.
6 A. Merenda, S. A. Orr, Y. Liu, B. Hernández Garcia, A. Osatiashtiani, G. Morales, M. Paniagua, J. A. Melero, A. F. Lee and K. Wilson, ChemCatChem, 2023, 15, e202201224.
7 S. Xu, D. Yu and P. Tian, RSC Adv., 2017, 7, 1026–1031.
8 M. M. Antunes, A. F. Silva, A. Fernandes, F. Ribeiro, P. Neves, M. Pillinger and A. A. Valente, Front. Chem., 2022, DOI:10.3389/fchem.2022.1006981.
9 Y. Kuwahara, W. Kaburagi, Y. Osada, T. Fujitani and H. Yamashita, Catal. Today, 2017, 281, 418–428.
10 S. S. Enumula, V. R. B. Gurram, M. Kondeboina, D. R. Burri and S. R. R. Kamaraju, RSC Adv., 2016, 6, 20230–20239.
11 R. Bao, S. Wang, J. Feng, Y. Duan, K. Liu, J. Zhao, H. Liu and J. Yang, Energy and Fuels, 2024, 38, 8437–8459.
12 V. V Sychev, Y. N. Zaitseva, A. O. Eremina, O. V Shabanova, S. D. Kirik, V. N. Panchenko and O. P. Taran, Chemistry, 2022, 15, 137–155.
13 Y. H. Zhou, Y. J. Luo, Y. T. Lin and Y. B. Huang, ChemistrySelect, 2018, 3, 11071–11080.
14 S. Kumaravel, S. Thiripuranthagan, M. Durai, E. Erusappan and T. Vembuli, New J. Chem., 2020, 44, 8209–8222
15 R. Zhao and J. W. Bae, Catal. Today, 2024, **435**, 114718.
16 J. He, H. Li, Y. Xu and S. Yang, Renew. Energy, 2020, **146**, 359–370.